Identification of the 1SXPS catalog sources discovered by the *Swift*-XRT

Daria Primorac

Supervisors: dr. sc. Olivier Godet and izv. prof. dr. sc. Dejan Vinković

Split, September 2015

Master Thesis in Physics

Department of Physics
Faculty of Science
University of Split

Title: Identification of the 1SXPS catalog sources discovered by the *Swift*-XRT

Author: Daria Primorac

Advisors: Dr.sc Olivier Godet
Dr.sc Dejan Vinković

Date: September 28, 2015

Abstract: Studying compact objects (CO) such as white dwarfs (WDs), neutron stars (NSs) and stellar-mass black holes (BH) with masses typically ranging from $3 - 20\ M_{\odot}$ is important for understanding the endpoints of stellar evolution and accretion/ejection processes, ubiquitous phenomena in the Universe. It provides further insights into the gas state and distribution in the early Universe. Studying the cosmic history of supermassive BH (with masses ranging from $10^{6-10}\ M_{\odot}$) growth could shed light on the formation and evolution of galaxies. It tells us more about their role in the reionization of the Universe and their impact on their (interstellar and/or intergalactic) environment. COs are also excellent laboratories to study matter in extreme conditions, such as matter at super-nuclear density in the NS interior or matter under the effect of strong gravity and magnetic fields in the vicinity of BHs and NSs, respectively. Due to accretion of matter that goes on in their vicinity, most COs were first detected in X-rays. For these reasons, all-sky X-ray surveys are most suitable for finding and studying such sources.

The *Swift* observatory, in operation since 2004, carries an X-ray telescope (XRT) and two other co-aligned instruments, the Burst Alert Telescope (BAT) and the UV/Optical Telescope (UVOT). This enables a multi-wavelength study of CO behaviour from optical to hard X-rays. *Swift* is dedicated to the study of gamma-ray bursts that appear randomly on the sky. This implies that *Swift* pointings have been performed all over the sky, covering 1905 square degrees with the XRT, with many fields observed several times within a day, over a period from many days to weeks/months (or even years), allowing to probe variability on various time scales.

In this work, I investigated the nature of the X-ray sources contained in the *Swift*-XRT catalog in order to isolate interesting objects possibly harbouring an accreting compact object (e.g. X-ray binaries, active galaxy nuclei – AGN, ultra-luminous X-rays sources, tidal disruption events). To do so, I cross-correlated a subsample of the *Swift* X-ray Telescope Point Source (1SXPS)

catalog, containing 98,762 sources with detections of best quality, with 16 external multi-wavelength catalogs which provide source type identification (active galactic nuclei, stars, X-ray binaries etc.) using the Topcat software. This enabled me to build a golden sample of known objects, divided into three main classes (AGNs, COs and stars) that represent the main types of objects observed in the X-ray sky. Within this subsample, I found that it consists of 4929 AGNs, 1125 stars and 231 COs. I studied their temporal, spectral and spatial properties in order to define selection criteria which would enable me to classify the rest of the 1SXPS sources. I found that COs are the most variable group, followed by AGNs and stars. Using spectral indicators from the 1SXPS catalog (power-law photon index Γ_{PL} and hardness ratios), I found that the Γ_{PL}-distributions of COs, AGNs and stars differ. For AGNs, the Γ_{PL}-distribution is clustering around 1.71, which is consistent with typical values derived for these objects. For COs, the distribution of Γ_{PL}-values is more widely spread, likely corresponding to the different spectral states that can be seen in X-ray binaries. Stars also display scattered Γ_{PL}-distribution, but with generally high values, implying that the PL model is not physical and that thermal emission is more likely. I found that most stars can be isolated from the rest of AGNs and COs thanks to their low X-ray to optical or IR flux ratio.

After establishing the selection criteria, I applied them to the golden sample of identified sources, in order to investigate the reliability of the defined selection scheme. 73% of the stars, 35% of the COs, and 95% of the AGNs were retrieved, with false classification probability of 8%, 78% and 15%, respectively. The low number of retrieved COs and their high probability of false identification is due both to the large fraction of AGN with respect to COs in the golden sample and the fact COs and AGNs share similar properties (Γ_{PL}-distribution and X-ray to optical/IR distribution intervals coincide). Finally, the selection criteria were applied back to the rest of the 1SXPS source high quality sample, resulting in 78,918 AGN candidates (86%), 9294 star candidates (10%) and 3752 CO candidates (4%). I discuss the caveats of the method used and I propose possible improvements, in particular for helping decreasing the high probability of false identification rate for COs. I also discuss further interesting works that could be done from the obtained results.

Keywords: Swift, AGN, compact objects, stars, X-rays, catalogs, accretion, X-ray binaries, multi-wavelength, cross-correlation

Acknowledgements

First, I would like to thank my supervisors, Dr.sc. Olivier Godet and my advisor in Croatia, Dr.sc. Dejan Vinković, for all their help and guidance. I would also like to thank the Erasmus organization for providing financial support for my visit to the University Paul Sabatier and the IRAP. Special thanks go to my colleagues Ante Rubić and Petra Žeko for their help and pieces of advice regarding the graphical representation of the results.

I am pleased to acknowledge that this work made use of data supplied by the UK Swift Science Data Centre at the University of Leicester (UK) and the use of the VizieR catalog access tool, CDS at Strasbourg (France) together with the cross-match service it provides. I also acknowledge the use of data products from the Two Micron All Sky Survey, which is a joint project of the University of Massachusetts and the Infrared Processing and Analysis Center/California Institute of Technology, funded by the National Aeronautics and Space Administration and the National Science Foundation.

Contents

List of Figures

List of Tables

List of Abbreviations

1SXPS	*Swift*-XRT Point Source catalog
AGN	active galaxy nuclei
APEC	Astrophysical Plasma Emission Code
ATHENA	Advanced Telescope for High ENergy Astrophysics
BAT	Burst Alert Telescope
BH	black hole
BHB	black hole binary
CbXb	Catalog of Cataclysmic binaries, Low-mass X-ray Binaries and Related Objects (7th Edition, Ritter & Kolb 2014)
CO	compact object
CV	cataclysmic variable
DENIS	DEep Near Infrared Survey
FlE	flaring and eruptive star
FOV	field of view
GCVS	General Catalog of Variable Stars (Version 2013, Samus et al. 2009)
GI	Guest Investigator Program
GRB	gamma-ray burst
HIP	Extended Hipparcos Compilation (Anderson et al. 2012)
HR	hardness ratio
IMBH	intermediate mass black hole
IPAC	Infrared Processing and Analysis Center
IR	infrared
IRAS	InfraRed Astronomical Satellite
LEDA	Lyon-Meudon Extragalactic Database
LINER	Low-Ionization Narrow Emission Line Regions galaxy
NlSy1	narrow-line Seyfert 1 galaxy
NS	neutron star
OrV	Orion-variable
PL	power-law
PrS	pre-main-sequence star
QSO	quasi-stellar object or quasar

SIMBAD	the Set of Identifications, Measurements, and Bibliography for Astronomical Data
SMBH	super massive black holes
SNR	supernova remnant
St	star (other)
Sy1	Seyfert 1 galaxy
Sy2	Seyfert 2 galaxy
TDE	tidal disruption event
ToO	Target of Opportunity Program
TOPCAT	Tool for Operating on Catalogs And Tables
ULX	ultra-luminous X-ray source
UVOT	UV/Optical Telescope
Vr	variable star
VV13	Catalog of Quasars and Active nuclei (13th edition,Véron-Cetty & Véron 2010)
WD	white dwarf
XB	X-ray binary
XRT	X-ray Telescope

1 Introduction

1.1 Compact object formation and detection

White dwarfs, neutron stars and black holes

Compact objects (CO) are the end points of stellar evolution, formed when the star runs out of fuel (or is not able to synthesise elements heavier than iron atoms by fusion reactions) and the collapse of their core occurs. The resulting type of stellar remnant is mainly determined by the mass of the progenitor star. In the case of a star with a core mass of $< 1.4\ M_{\odot}$ a white dwarf (WD) is formed (e.g., Anderson 1929; Chandrasekhar 1931). That makes them final remnants of low- and intermediate-mass stars. About 95% of main sequence stars will end their evolutionary pathway as WDs. WDs have approximately the mass of the Sun and the size of the Earth. For instance, Sirius B has the mass of the Sun confined within a volume smaller than the Earth ($\approx 0.008\ R_{\odot}$), resulting in an average density of 3.0×10^9 kg m^{-3}, and the acceleration due to the gravity on its surface is about 4.6×10^6 m s^{-2}. The collapse of the stellar core is stopped by the electron degeneracy pressure. Indeed, electrons (being fermions) obey Pauli exclusion principle. As they can not be in the same quantum state, the gravitational collapse that leads to an increase in electron density is eventually put to stop by degeneracy pressure (or equivalent, by the requirement of putting electrons at higher energy levels). After formation, the WD evolution can be described as a simple cooling process, which is reasonably well understood (Salaris et al. 2000; Fontaine et al. 2001). In the case of more massive stars, evolution is more complicated, since electron-degeneracy is not able to

sustain the gravitational forces and further collapse occurs. If the stellar core is between 1.4 and $2.2-2.9\ M_{\odot}$, depending on the core angular momentum, the gravitational collapse will be stopped again due to the Pauli exclusion principle, but only after the neutron-degenerative matter is formed. As the core shrinks, its density will rise until it reaches nucleonic values $\sim 10^{12} - 10^{14}$ g cm^{-3}, at which point protons will start capturing electrons to transform into neutrons, resulting in emission of neutrinos (e.g., Epstein 1979; Bethe & Wilson 1985; Bethe 1990). The existence of such objects, called neutron stars (NS) was proposed two years after the discovery of the neutron in 1932 (see Baade & Zwicky 1933; Landau 1932). Given that the radius of a 1.4 $M_{\odot}$ NS lies roughly between 10 and 15 km (depending on the NS equation of state), the average density in the core of NSs would be equal to 6.65×10^{17} kg m^{-3}, greater than the typical density of an atomic nucleus (see Oppenheimer & Volkoff 1939 for first models of NSs). The nature of the matter in the core of NSs is still unknown, but could provide important insights to find the elementary constituents of matter. Above the NS mass limit (stellar core with mass $> 2.9\ M_{\odot}$), there is no force in Nature able to stop further gravitational collapse. The object formed is called a black hole (BH – Oppenheimer & Snyder 1939) because even light can not escape from the hole gravitational well. BHs are only described by their mass and their spin. Assuming an escape velocity equal to the speed of light c, a simple Newtonian calculation gives a radius equal to $R_S = 2GM/c^2$, called Schwarzschild radius (Schwarzschild 1916). In terms of the mass of the Sun, $R_S = 2.95\ (M/M_{\odot})$ km. The spherical surface at $r = R_S$ (called the event horizon) then acts as a barrier and prevents us from receiving any information from below this radius.

In principle, isolated NSs and WDs will be faint and therefore not easily detectable (although, there are exceptions such as isolated NS called magnetars – NSs in which the main source of energy is provided by a strong magnetic field, instead of accretion or nuclear reactions, see Kouveliotou 1999) while non-accreting BHs will not be visible at all, since they do not emit radiation. Still, dormant BHs can be detected through other methods such as stellar kinematics or gravitational lensing. Although as many as

one-quarter of stars in the vicinity of the Sun may be WDs, the complete sample has been obtained only within very close distances from the Sun. Holberg et al. (2008) presented a (probably) complete sample of local WDs within 13 pc and demonstrated that the sample becomes incomplete beyond that distance. More recently, a nearly complete sample up to 20 pc was provided (Giammichele et al. 2012). The astrophysical study of COs mainly relies on the detection of the emission, in particular in X-rays, induced by the accretion of matter in the vicinity of these objects (Pringle 1981). The nature of processes that occur in their vicinity, accretion of mass in a form of an accretion disk or a direct flow, has mass to energy transformation efficiency up to 0.4[1]. This is ten times greater than the efficiency of the nuclear burning of hydrogen, and as a result, energy is emitted in the form of X-rays. Accretion disks are commonly found when gas, with angular momentum, is gravitationally attracted towards a central massive body (Frank, King, & Raine 1992). Matter is transported inwards and angular momentum outwards, while causing the disk to heat up. The expected spectrum peaks at optical-ultraviolet waveband, but hot corona above the accretion disk also gives rise to the X-ray power-law spectrum via scattering processes. For this accretion disc to exist, either a donor star (in the case of binary systems), or material (in the case of active galactic nuclei) has to be present. As a consequence of this ubiquitous process in the Universe that releases a huge amount of energy in a rather confines space, COs are the main type of X-ray emitters and a large number of them was first detected by X-ray surveys.

Observations of the orbits of particles in the disc can be used to obtained information about the spacetime geometry near COs. Even at temperatures of $\sim 10^7$K that characterize the inner parts of an accretion disc, some heavy nuclei (such as iron) retain bound electrons. Incident radiation from X-ray flares occuring above and below the disc can lead to fluorescence from the highly ionised atoms in the disc (electron in the atom is de-excited from a higher energy level to a lower one and emits a photon). For iron atoms, this gives a spectral lines roughly in the middle of the X-ray band (6.4 – 7 keV). Emitted and measured photon energy differ. This frequency shift

[1]http://www.astro.utu.fi/ cflynn/astroII/l6.html

is caused by two effects: the photons will be gravitationally redshifted (by an amount that depends on the radius from which they were emitted) and Doppler shifted (by an amount that depends on the speed and direction of the accretion flow relative to the observer). In the measured spectra of such objects, radiation at each frequency comes from various parts of the disc. The shape of the observed broadened iron line then contains information about the spacetime geometry around the accreting object (e.g., Brenneman & Reynolds 2006; Reynolds & Fabian 2008).

Cataclysmic variables and X-ray binaries

Cataclysmic variables (CVs) are a closely bound interacting binary system in which a WD, often referred to as the "primary" star, accretes material from its main-sequence companion called the "secondary" star (see Smith 2007 for a review on CVs). This interaction leads to a rich range of behavior. Depending on the intensity of the magnetic field of the WD, accretion can occur through an accretion disk for a weak or nonexistent magnetic field or through flow channeled directly onto the magnetic poles in the case of magnetized WD (e.g., Balman 2011). As gas from the secondary star continues to fall towards the primary, it impacts the edge of the accretion disk creating a "hot spot" (Figure 1.1). As the secondary star loses material during this process, a fraction of the gravitational energy released by the accreted matter is converted to radiation, particularly in X-rays within the inner parts of the accretion flows. This process will begin once the secondary star overfills its Roche-lobe, a potential surface that passes through the inner Lagrangian point L1. In other words, the Roche-lobe surface is the location between two stars in a binary, where the gravitational pull from one star is equal and opposite to that of the other star. This point (L1) of unstable equilibrium can occur near the surface of the secondary if the orbital radius is small, as it is the case for CVs which usually have orbital periods less than half a day with separation distances between the two stars typically less than a few solar radii (Smith 2007). With one star filling its Roche lobe, the system is said to be semi-detached. Contact of the inflow material with the WDs surface lead to outbursts, which differs from system to system in the

released amount of energy and the recurrence time, ranging from weeks or years to the $10^4 - 10^5$ years, depending on the CV class. These objects are fairly faint in X-rays (with X-ray luminosity $L_{\rm X} \sim 10^{33}$ erg s^{-1}), compared to X-ray binaries (XB). Some works consider CVs as a special class of XBs (Balman, 2011).

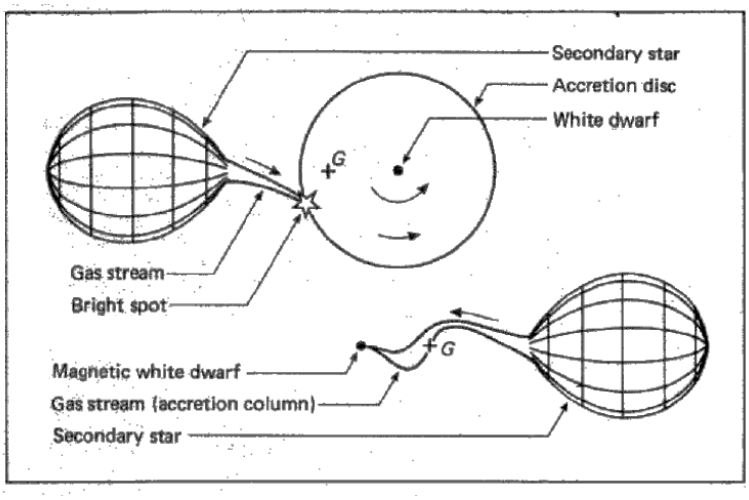

Figure 1.1: Model of a CV: a cool red secondary star and a WD orbit around their common centre of mass (G). Top - In non-magnetic systems, there is an accretion disc with the bright spot, created by the impact of the gas flow from the secondary star. Bottom - Magnetic field of a WD directs the gas stream along field lines onto the WD. Taken from Pringle & Wade (1985).

XBs are accreting binary systems with the primary star being a NS or a stellar mass BH. Because of the higher mass of the primaries, separation between the two stars can vary on larger scale than for CVs. The first strong evidence for a stellar-mass BH came from the X-ray and optical observation of the XB Cygnus X-1 (Bolton 1972; Webster & Murdin 1972), as it was known that the blue supergiant observed in optical should not be the source of strong detected X-ray radiation. Furthermore, its motion suggested that it is orbiting a very massive compact object. The second BH candidate identified was LMC X-3 (Cowely et al. 1983), also in X-rays. The third identified black hole binary (BHB) was discovered as an X-ray nova

in 1975 when it suddenly became the brightest non-Solar X-ray source ever observed in those times (Elvis et al. 1975). Nearly all BHBs appear as X-ray novae that were discovered when they first went into outburst. During the outburst phase the source radiates an amount of radiation (in particular in X-rays) several orders of magnitude larger than when it is in quiescence. The outburst phase is thought to be the result of an instability that arises in the accretion disc (e.g., Remillard & McClintock 2006). In the overview of BHBs Remillard & McClintock (2006) show that over 20 X-ray binaries containing a dynamically-confirmed BH, only three of them are persistent X-ray sources. Also, half of these BHBs are now known to recur in outburst on timescales of 1 to 60 years, where the outburst amplitude as well as the outburst frequency can vary strongly from source to source and within a given source. As most of XBs are then in quiescence between outbursts, their discovery relies on serendipitous detections thanks to X-ray surveys, covering large parts of the sky, with a particular interest in the direction of the Galactic Center where, given the density of stars, a large number of XBs can still be found. The observed diversity is shown in Figure 1.2.

Long period systems and short ones differ in their secondary star, hot or cool supergiant in contrast to the K-dwarf star. Mass function that puts some constrains on the BH mass can be simply determined by measuring the radial velocity curve of the secondary star. But, that observational quantity is not always available due to the lack of optical counterpart for many of these systems. Also, they could be difficult to measure, depending on the inclination of the system with respect to the line of sight. Still, they are considered an BHB candidates because of the close similarities in their X-ray spectral and temporal behavior when compared to the confirmed ones. The evolution of these transient sources is complex, but there are behavior patterns common to all of them. In basic we distinguish two states, the high/soft state usually observed when the source is bright, and the low/hard state observed when the source is faint, characterized with a higher and a lower power-law photon index, respectively (Remillard & McClintock 2006). These variation in the X-ray luminosity by 5 – 8 orders of magnitude and

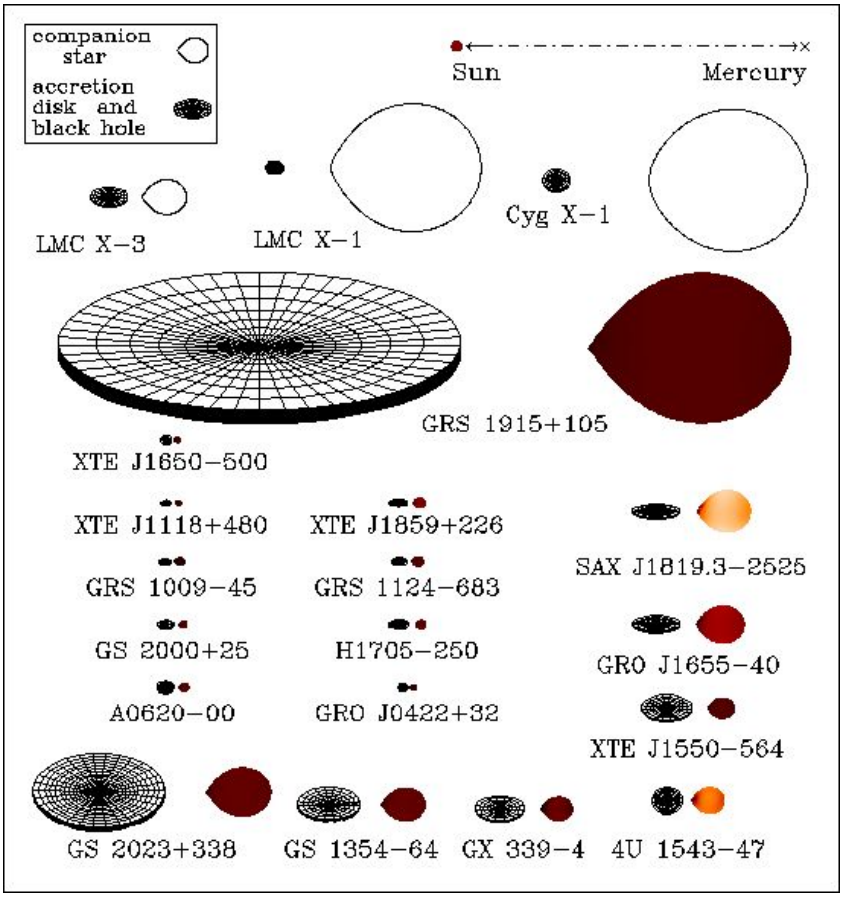

Figure 1.2: Scale drawings of 16 black-hole binaries in the Milky Way, where the color of the companion star is the indicator of the surface temperature. The Sun-Mercury distance is showed for scale in the top right corner. Tilt of the accretion disk indicates the estimated binary inclination. Image taken from the Remillard & McClintock (2006).

the described periodic transient behavior on the long time scales call for an ongoing observations as well as a rich X-ray data archive. XBs are also known to display radio jets in some spectral states associated with matter ejection episodes. The physical mechanisms to launch these jets are still poorly understood.

Active galactic nuclei

Of interest are also the BHs on the other end of the mass scale, known as super massive black holes (SMBHs), with masses ranging from 10^6 to 10^{9-10} $M_\odot$, located in the nucleus of most massive galaxies (Magorrian et al. 1998; Richstone et al. 1998; see Ho 2008 for a review). Accreting SMBHs are known as active galactic nuclei (AGNs), which emit a large amount of emission over all the electromagnetic spectrum (with bolometric luminosity $L_{\rm bol} \sim 10^{43-47}$ erg s^{-1} – e.g., Woo & Urry 2002), sometimes accompanied with powerful outflows of energetic particles and radio emission. With nucleus so bright that it overpowers the emission from billions of stars in their host galaxy, AGNs can be seen across the Universe. SMBHs with 10^9 solar masses have been identified at distances corresponding to a light travel time of more than 12 billion years, meaning that they had to grow very quickly (Fan et al. 2001). Some theories (see Section 1.3) proposed that they were formed through the accretion episodes and/or merger of lighter seeds formed in the early Universe, the so-called Intermediate Mass BHs (IMBH – see Miller & Colbert 2004 for a review on their possible formation paths and where we may expect to find them).

Many of the apparent differences between types of AGNs are thought to be due to their different orientations along the observer line of sight, as shown in Figure 1.3. This is known as the AGN paradigm (e.g., Antonucci 1993; Urry & Padovani 1995). The continuum emission coming from the central engine is well modeled by a power-law with an average value of photon index $\Gamma_{PL} = 1.9$, with typical variation over $\Gamma_{PL} \sim 1.7 - 2$ (Corral et al. 2011; Caccianiga et al. 2004; Nandra & Pounds 1994). The central engine is thought to be hidden, for some particular observer lines of sight, by an obscuring medium located around it, often referred to as a "torus". So, when observed on the sides, the central source is no longer visible along the observer line of sight. In that case the soft X-ray radiation is absorbed and only the hard X-ray could escape and be observed. This is known as Type-II AGN. Also, sometimes the light from the central engine could be reflected by materials located somewhere above the disk in the direction of the observer, leading to a soft component (Done et al. 2011). Fluorescence

$K\alpha$ and $K\beta$ lines produced by neutral or ionized iron atoms present in the material obscuring the central source could also be detected. As the viewing angle decreases, the central engine becomes totally or partially visible. These AGNs are referred to as Type-I AGN. They often present strong soft excess that corresponds to redistributed emission produced by a warm absorber (clouds of gas photoionized by the continuum emission from the central source) found above the disk, in addition to the continuum coming from the central engine (Singh et al. 1985; Turner & Pounds 1989). More precisely, in the X-ray domain, for a neutral hydrogen column density N_H in the line of sight smaller than 10^{22} cm^{-2}, AGN is classified as Type-I, and for larger values as Type-II (Treister & Urry 2005). Type-II AGN show steeper Γ_{PL}-values ($\Gamma_{PL} \sim 2.0 - 2.2$) than Type-I AGN ($\Gamma_{PL} \sim 1.5 - 1.8$). Type-I AGN can be further classified as Seyfert 1 or quasar (QSO), depending if the host galaxy is clearly detectable or if it is seen as a point-like object. There are many more subclasses depending on the degree of the viewing angle, spectral characteristics, etc. For example, BLLac objects are AGNs whose relativistic jets are aligned with the observer line of sight, while LINERs (Low-Ionization Narrow Emission Line Regions) display strong low- ionization lines in their emission spectra relative to its high-ionization lines. In the local Universe, obscured AGNs are seen to be more common than unobscured AGNs by a factor of $\sim 3 - 4$ (Risaliti et al. 1999). Observations in hard X-rays (>2 keV), that can penetrate the obscuring material, are therefore necessary for the observation of the hidden nuclei.

Tidal disruption events and black hole detection signatures

Not all galaxies that contain a SMBH are necessary active, due to the lack of material that can be accreted. The SMBH is then said to be in quiescence. This can change if a star wanders too close to the SMBH. If the star approaches at a distance less than the tidal radius, at which point strong tidal forces exceed the self-gravity of the star and disrupt it. In that process, $\sim 1/2$ of the star mass stays bound to the hole while the remaining is unbound and will espace (e.g., Gurzadian & Ozernoi 1981; Rees 1988; Ulmer 1999; Strubbe & Quataert 2009). In the end, as little as 10% of the total

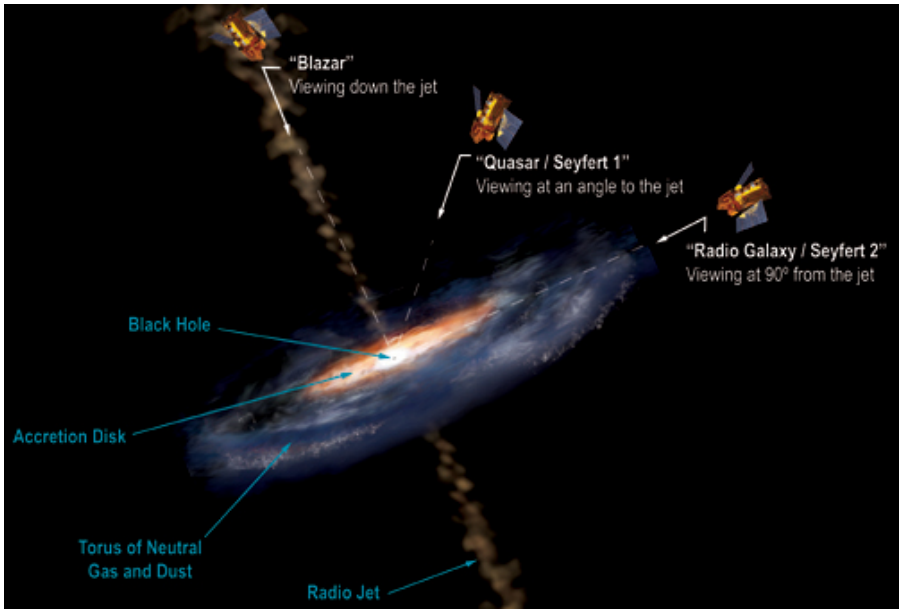

Figure 1.3: Type of the observed AGN depending on the different orientations along the observers line of sight. Taken from `http://www.nasa.gov/centers/goddard/news/topstory/2007/active_galaxy.html`.

mass of the star may be accreted (Ayal et al. 2000). These tidal disruption events (TDEs) produce luminous UV/soft X-ray emission peaking shortly after the disruption took place (sometimes, depending on the structure of the star, the impact parameter and the BH mass, the star can be "swallowed " completely before ever being disrupted). After the peak, emission decreases in flux at a rate $t^{-5/3}$, over timescales of weeks or years in otherwise inactive galaxies (Komossa & Greiner 1999; Grupe et al. 1999). An example of such light curve decline is shown in Figure 1.4. These events then offer a way to probe the presence of a SMBH in inactive galaxies together with its mass and spin, independent of locally established scaling relations between the central BH mass and its host galaxy properties (Gebhardt et al. 2000; Ferrarese & Merritt 2000; Graham et al. 2001). They also could help in better understanding the BH occupation fraction in low-mass galaxies, important for the early Universe seed model (e.g., Greene 2012). Predicted TDE rates are low, about 10^{-3} to 10^{-6} yr^{-1} per galaxy, depending on the

stellar density and the SMBH mass (Wang & Merrit 2004). Only about a dozen of TDE candidates have been identified so far in X-ray (Komossa 2002; Donley et al. 2002; Esquej et al. 2008; Cappelluti et al. 2009; Maksym, Ulmer, & Eracleous 2010; Lin et al. 2011; Saxton et al. 2012) observations. All-sky X-ray surveys are best suited to detect such events. Indeed, TDEs were first discovered with *ROSAT* observatory (Bade et al. 1996, Komossa & Bade 1999), due to its soft X-ray sensitivity, all-sky coverage and long lifetime. The *Swift* observatory shares these characteristics and it's also ideally suited for detection of these events. Because of its multiwavelength capabilities, it can provide additional information about optical and ultraviolet counterparts (e.g., Rees 1988; Ulmer 1999; Strubbe & Quataert 2009). For example, the unusual transient source detected with the *Swift* observatory (Swift J164449.3+573 – see Figure 1.4) at the center of a compact galaxy ($z \simeq 0.353$), is thought to be a result of the relativistic outflow, powered by accretion following the TDE of a star by a SMBH (Bloom et al. 2011; Burrows et al. 2011). TDEs also occur in AGNs, but their identification can be challenging, due to the low luminosity contrast between permanent accretion disk and temporary TDE flare and due to the number of mechanisms in the reservoir of obscuring material that can mimic large amplitude-variability. More observations of TDEs in non-active galaxies is then needed for determining the precise behavior of X-ray spectral and temporal evolution, in order to pinpoint TDEs in AGNs.

BHs can be detected by distinctive signatures associated with accretion process. Interactions between photons and electrons form an X-ray corona above the accretion disk. The region is very compact, but the variability can be observed on a wide variety of time scales, from milliseconds to months (see Figure 1.5). Although variability is not intrinsic to the accretion disc around a BH, it can be distinguished from the accreting NS not only by mass measurement, but also by their larger variation in luminosity between their bright and faint states, when compared to the accreting NS (Narayan et al. 1997). Another signature comes from fast-moving gas orbiting the BH outside the accretion disk. Because of the high velocities, observed spectral line transitions are shifted to the blue or the red via Doppler effect (thus the

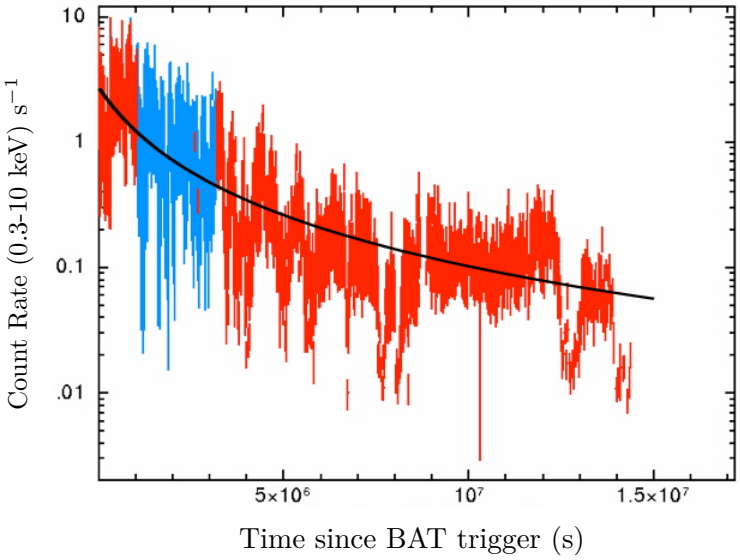

Figure 1.4: The *Swift*-XRT light curve of Swift J164449.3+573, fitted using a simple $t^{-5/3}$ law (solid black line). Different colors of the light curve correspond to different modes of XRT operation. Taken from Lodato (2012).

name "broad-line" region – see Figure 1.6 on the left). Finally, the gas in the galaxy on larger scales is excited by the emission from the accretion disk. Ratios of different atomic transitions form a specific fingerprints that can be observed in ultraviolet, optical, near-infrared and mid-infrared wavelengths (e.g., Ho et al. 1997). For instance, a reliable indicator of AGN activity detected in mid-infrared spectroscopy is the high ionization [Ne V] line, as starlight likely cannot excite this transition (e.g., Satyapal et al. 2007). For relatively nearby galaxies, the existence of SMBHs can be detected more directly, namely by looking at star motions near the galaxy center. Stars near the center will move faster on average if the SMBH is present (see Figure 1.6 on the right). Star motion near the SMBH tends to blur together with motion of more distant stars that don't feel its influence, meaning distance to the galaxy plays an important role. Using similar principles, orbiting gas clouds can also give away the presence of a SMBH (e.g., Barth et al. 2001; Herrnstein et al. 2005; Kuo et al. 2011). At the center of our own Milky Way galaxy, motion of individual stars can be traced. Early observations of

gas motion in the Galactic center suggested a strong concentration of mass (e.g., Lacy et al. 1980; Genzel et al. 1985). Then, multiple stellar orbits have been tracked around the $\sim 3 \times 10^6 M_\odot$ BH in the center of our Galaxy (e.g., Eckart & Genzel 1996; Ghez et al. 1998; Ghez et al. 2000).

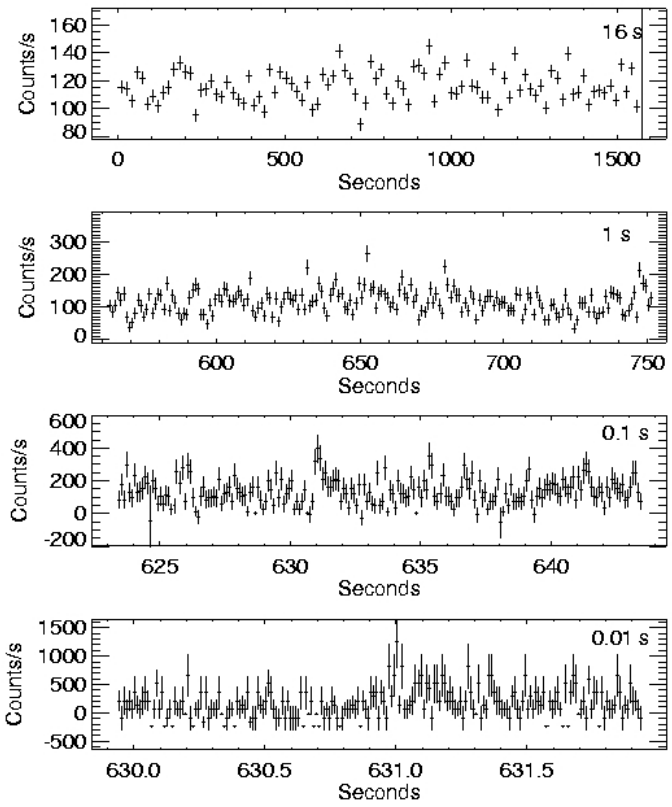

Figure 1.5: The 16-, 1-, 0.1-, and 0.01-second time resolution light curves of the Galactic BH candidate GRS 1758+258. Taken from Lin et al. (2000).

Ultraluminous X-ray sources

Specially interesting then in the field of astrophysics are very bright sources that do not lie inside the nucleus of their host galaxy. Ultraluminous X-ray sources (ULXs) are defined as extragalactic objects located outside the nucleus of the host galaxy with bolometric luminosities that exceeds

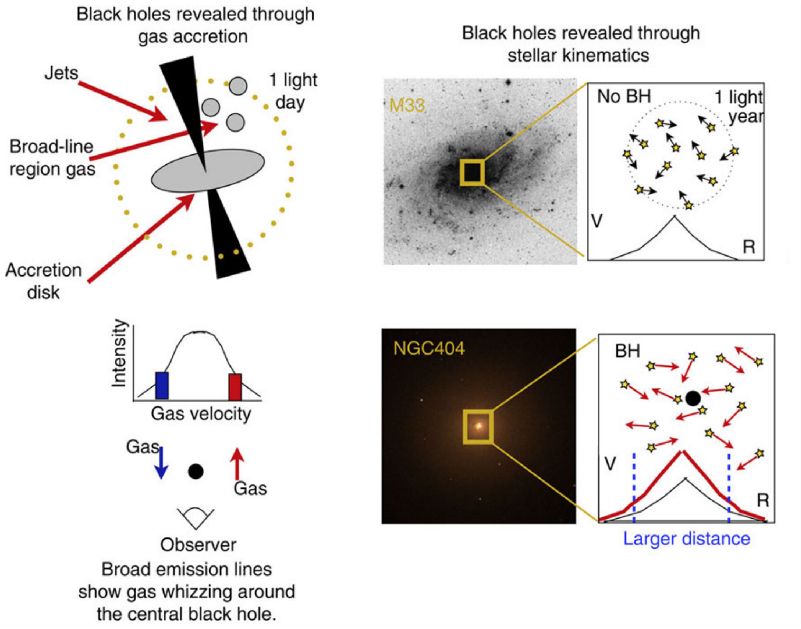

Figure 1.6: Schematics of SMBH detection. Left - Detecting accretion onto BH through accretion and the Doppler shift of orbiting gas in the broad-line region. Right - Direct BH detection with stellar kinematics. Taken from Greene (2012).

10^{39} erg s^{-1} (Roberts 2007). It is generally accepted that they can not host BHs as large as those associated with AGNs, as they would sink into the central galactic gravitational well due to dynamical friction (e.g., Miller & Colbert 2004) within the Hubble time, and again they appear to be significantly more luminous than X-ray binaries (Walton et al. 2011). They are thought to be powered by accretion onto BHs. But, because of the extreme luminosities (that exceed the Eddington limits for a 20 $M_{\odot}$ stellar mass BHs), the ULXs would need to be 10 – 100 more massive (Colbert & Mushotzky 1999). The existence of such intermediate mass black holes (IMBHs), that would fill the gap between the stellar BHs and supermassive ones, is still in dispute (see the general reviews in van der Marel 2004; Rasio et al. 2006). There are many proposed candidates, but non are accepted as definite. The brightest ULX in the galaxy ESO 243-49, HLX-1,

is the strongest candidate to harbour an IMBH with a mass estimate from 9000 to 90,000 $M_{\odot}$ to date (Godet et al. 2012; Straub et al. 2014; Servillat et al. 2011; Davis et al. 2011). So, the detection of new ULXs with X-ray luminosity larger than 10^{41} erg s^{-1} could offer a way to find other IMBH candidates. There are two other possibilities that could explain such extreme luminosities. First one is the idea that ULXs do not emit isotropically, and we observe them at favorable orientation. Luminosity is usually calculated under the assumption of isotropy, so in the case of anisotropy this can lead to overestimation of the source luminosity (e.g., King et al. 2001). Then there would be no need to invoke larger BH mass than the ones found in stellar mass BHBs. Recently, the masses of two ULXs were dynamically measured to be in the stellar-mass BH range (Liu et al. 2013; Motch et al. 2014). The other possibility also does not rely on the existence of the IMBHs. Instead, it suggests that the accretion state of these stellar mass BHBs is such that they are able to accrete above the Eddington limit (above which radiation pressure forces exceed gravitational attraction, blowing away accreting gas). A large fraction of ULXs harbours probably a stellar mass BH (Feng & Soria 2011). Detection of a known BHB located in M31 emitting above 10^{39} erg s^{-1} may suggest that ULXs could be BHBs seen in an extreme hyper-critical state (Middleton et al. 2013), the so-called ultraluminous state (see also Gladstone et al. 2009 and citations). Monitoring of the known ULXs will provide further insights into differences between them and confirmed BHBs. Also, recent data analysis of ULX in M82 indicated that the compact object is likely to be a NS accreting to 100 times the Eddington limit (see Bachetti et al. 2014). Regardless of the ULX true nature, they are of great interest for X-ray surveys. IMBHs could have played important role in the formation of the SMBHs in the early Universe. On condition that ULXs are NSs or stellar mass BHs, then these extreme luminosity objects would present a good laboratories for the study of the hyper-accretion physics (e.g., Feng & Soria 2011).

1.2 X-ray surveys overview

Since Earth's atmosphere blocks out X-rays, only a telescope in space can detect and be used to study celestial X-ray sources. In addition, observations in optical are performed by big and medium-sized telescopes on Earth, which are not suitable for the rapid follow-up needed for the study of transient sources. Due to the small-size scales of emitting regions involved in the accretion process, the resulting X-ray emission is often highly variable and related transient events that occur are typically short of duration (from few days to a fraction of a second). Smaller telescopes in orbit around Earth, with their independence of atmospheric conditions, observing flexibility and rapid response and slew times are then very well suited for finding and continuous monitoring of these sources. Numerous observations of the sky in X-rays have being carried out by observatories such as *Einstein Observatory* (Giacconi et al. 1979), *ROSAT* (Trümper, 1983), *XMM-Newton* (Jansen et al. 2001) and, since 2004, by the *Swift* mission (Gehrels et al. 2004). Serendipitous X-ray sources detected by these observatories provide essential pieces of information for understanding the X-ray sky, especially the nature of COs.

Before the launch of the *Einstein Observatory* in November 1978, only four galaxies, if bright X-ray sources associated with Seyfert nuclei are excluded, had been detected in X-rays: the Milky Way, M31, and the Magellanic Clouds. The *Einstein Observatory* was the first imaging X-ray telescope, and its observations produced revolutionary leap in our understanding of the X-ray sky. The *Einstein* images, in $\sim 0.2 - 3.5$ keV range, with spatial resolution of 5 arc seconds gave the first clear detection of individual X-ray sources in nearby spiral galaxies, resolving their compact sources distribution and discovering the first ULXs (Fabbiano 1989) in more distant galaxies. Super-winds from actively star-forming galaxies were also first discovered with *Einstein*, as were the hot diffuse halos in elliptical galaxies (see Fabbiano 1989 Annual Review article on the X-ray emission from galaxies). Increment in number of observations, improvements of limiting sensitivity and/or angular resolution came with subsequent X-ray observa-

tories, expanding our knowledge of the X-ray properties of stars, galaxies and COs.

ROSAT, one of the following X-ray missions, performed the first ever all-sky survey, producing a catalog containing $\sim 90,000$ X-ray sources. Some of the discoveries included the detection of isolated NS and X-ray radiation coming from comets, but only with *Chandra X-ray Observatory* (Weisskopf et al. 2000), launched on July 23 1999, and its subarcsecond spatial resolution, X-ray observation of the sky has taken a second revolutionary leap, opening up the field of X-ray population studies in galaxies. Population studies are often used in astronomy, to both constrain the physical characteristics of a class of sources and to study their evolution. Prior to *Chandra*, the study of the properties of the X-ray sources within the galaxy had to be restricted to most nearby ones. X-ray population studies are best done outside the Milky Way (Fabbiano 1995), providing a complete sample of X-ray sources, without the biases in distance and line of sight absorption immanent to Galactic source studies. With *Chandra*, populations of individual X-ray sources, with luminosities comparable to those of Galactic XRBs, can be detected at the distance of the Virgo Cluster and beyond, and the emission of these sources can be separated from the diffuse emission of hot interstellar gas (see Fabbiano 2002 for a review on the observations of galaxies with *Chandra*). To illustrate how higher resolution can reveal new features, the two images of the Crab Nebula and its pulsar are shown in Figure 1.7, where on the left it is a *ROSAT* image, the observatory with the best imaging capability before *Chandra* (right).

Launched just a few months after Chandra was the *XMM-Newton Observatory* (Jansen et al. 2001), which has, since then, produced the largest X-ray source catalog thanks to its large effective area. In the latest released version 3XMM - DR5 (Rosen et al. 2015), there are 565,962 X-ray detections comprising 396,910 unique X-ray sources. For comparison, the *Chandra* source catalog (Evans et al. 2010) included information for about 94,676 distinct X-ray sources. A few examples of the contributions of *XMM-Newton* to the understanding of the X-ray sky include: determining that Milky Way's BH have possible been woken up violently about 400 years ago

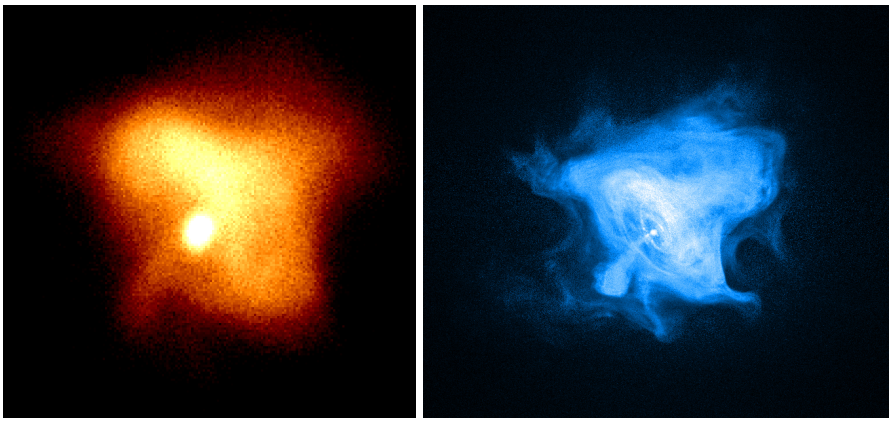

Figure 1.7: Left - Crab Nebula and Pulsar observed by the *ROSAT* High Resolution Imager in 0.1 – 2.0 keV range. Right - Image of the same source taken by the *Chandra* Advanced CCD Imaging Spectrometer in 0.5 – 8.5 keV, with fifty times better resolution than the one on the left. *ROSAT* Credit: S.L. Snowden, NASA/GSFC. *Chandra* Credit: NASA/CXC/SAO.

and then turned off again about 100 years later, acquiring the first large-scale map of the dark matter and baryon distributions in the Universe and measuring the spin state of SMBHs for the first time. *XMM-Newton* has also showed that winds from a SMBH blow outward in all directions and for the first time detected a switching X-ray emission from a highly variable pulsar (see Santos-Lleo et al. 2009 for a review on the first decade of observations with *Chandra* and *XMM-Newton*). There were many more X-ray observatories launched by this date, including the *Swift* mission, of which the serendipitous X-ray source catalog was used in this work. The mission and the catalog are discussed in more detail in Chapter 2.

1.3 Studies of compact objects

How did ordinary matter assemble into the large scale structures we see today? How do BH grow and shape the Universe? These are two leading opened questions for the forthcoming years. Indeed, large scale structures grow over cosmic time by accretion of gas from the intergalactic medium,

with todays massive clusters of galaxies, the largest bound structures in the Universe, being the endpoint of their evolution. Except by the large scale dark matter distribution, this growth is affected by processes of astrophysical origins (Pointecouteau et al. 2013; Ettori et al. 2013; Croston et al. 2013), one of the critical being the energy input commonly known as feedback from SMBHs (Croston et al. 2013; Cappi et al. 2013; Fabian et al. 2009). Seemingly, processes originating close to the BH seem able to influence structures on scales 10 orders of magnitude larger (Cappi et al. 2013; Dovciak et al. 2013). Jets of accelerated particles that emit radio photons often accompanies accretion processes, although the exact launching mechanism is still poorly understood. Winds and jets from AGNs can interact with their surroundings. This can lead to ejection or heating of the gas and as a consequence quench star formation in the galaxy and stifle accretion onto the black hole (e.g., Fabian 2012). X-ray observations are essential to further progress in understanding this processes.

We can not have a complete understanding of galaxies without understanding how their central SMBHs grew through cosmic time, and how they formed to begin with. Theoretically, two models have been proposed. Either first BHs formed in the same way they do today, as the end-product of stellar evolution (leaving BH seed $\sim 100\ M_{\odot}$), or the BHs where made directly by the collapse of gas clouds (BH seed $\sim 10^4 M_{\odot}$). The former model requires massive stars (e.g., Bromm & Yoshida 2011; Heger et al. 2003) and the later requres high gas fractions with low angular momentum and low metallicities in the early Universe (e.g., Haehnelt & Rees 1993). The growth of these seeds into SMBH observed only a few hundred million years after the Big Bang (Fan et al. 2001) is also described by different models, including accretion at Eddington limit, mergers of smaller BH seeds (e.g., Li et al. 2007) or mergers of stars, forming a supermassive star leading to the formation of a more massive seed (e.g., Portegies Zwart et al. 2004; Devecchi & Volonteri 2009). Assuming that growth was accomplished by a combination of accretion and mergers, the sheer number of left-overs should indicate the correct formation scenario (e.g., van Wassenhove et al. 2010). If BHs form similarly in all galaxies, then the number and masses of BHs in small galaxies

today can be used to distinguish between the two scenarios, since a higher fraction of low-mass galaxies (those with stellar masses $M_{gal} < 10^{10} M_{\odot}$) to contain nuclear BHs is invoked if seeds are created via stellar deaths (see Volonteri et al. 2008 and Figure 1.8). Still, there are many uncertain details associated with these models, such as whether the first stars formed in pairs or how much they lose mass during late stage of their evolution. Also, as BH merge, they emit gravitational radiation which can lead to gravitational "recoil" (Merritt et al. 2004), in some cases leading to the ejection of the BH out of the galaxy, but with, for now, unknown efficiency (see Greene (2012) and Volonteri (2010) for review of the leading theories for the formation of the first massive BHs).

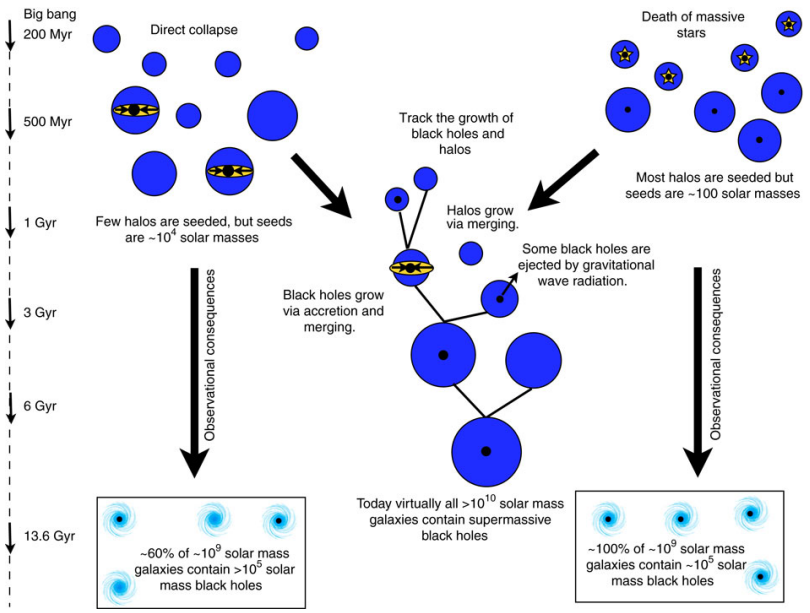

Figure 1.8: Schematic of the BH seed evolution assuming two different formation paths (the death of the first generation of massive stars vs. the direct collapse of gas into a BH), with different BH occupation fraction of low-mass galaxies as a result. Dark matter halos and the galaxies in them grow through merging while BHs grow both via merging and by accreting. Image from Greene (2012).

Unfortunately, as BH masses are tightly correlated with the mass and structure of their host galaxies (Ferrarese & Merritt 2000; Gebhardt et al. 2000; Graham et al. 2001), understanding the SMBH population becomes increasingly challenging as one considers lower and lower-mass galaxies. As central BHs in smaller galaxies are less massive, both their emission and gravitational force is weaker, making them harder to detect via accretion or stellar dynamics (see Section 1.1). Furthermore, cold gas, dust and higher levels of on-going star formation, all typically found to a larger extent in low-mass galaxies, obscure and mask emission coming from accretion. In the future, very sensitive X-ray surveys will enable us to search for accreting SMBHs in smaller galaxies over larger distances (Xue et al. 2011). One of the key goals of *ATHENA* (Advanced Telescope for High ENergy Astrophysics) *Observatory* (Barcons et al. 2012) is to observe the BH evolution at $z = 6 - 10$ redshifts, where the first galaxies were forming (Aird et al. 2013; Georgakakis et al. 2013). This will also yield the first detailed X-ray spectra of accreting BH at the peak of galaxy growth at $z = 1 - 4$, measurements which are impossible with current instrumentation. Until then, finding and sampling SMBHs in low-mass galaxies by exploiting current multi-wavelength catalogs, in particular in X-rays, is of key interest in order to get more insight on the global picture drawn above.

Demographic studies of stellar-mass COs are also of interest, as both past and on-going star formation can be explored by COs. The X-ray observations of such sources will allow astronomers to gain a better understanding of the end-point of stellar evolution for massive stars and how their collapse enriches the Universe with heavy materials. The SNR 1987A in the Large Magellanic Cloud has renewed theoretical interest in alternative models for the aftermath of a supernova explosion. It was the first time since the development of modern instruments that a supernova has been seen so close to Earth. Yet, as of 2006, neutrinos have been the only direct evidence of the CO formation at its center. The on-going failure to detect a young NS in the remnant supports model of a newborn NS that, under some circumstances, collapses into a BH shortly after birth (Brown & Bethe 1994; Woosley & Timmes 1996). In addition, efforts to find any evidence of a

surviving binary companion have also been unsuccessful. As the timescales over which the SMBHs are active are much too long for a complete scientific study, best opportunities to understand accretion and jet formation through spectral changes are likely to come from studies of transient stellar-mass COs. Stellar-mass accretors have relatively short variability timescales ranging from hours, days to years. Phenomena that arise in strong gravitational fields of COs gives us the opportunity to study and test fundamental physics (e.g., Psaltis et al. 2014; Huwyler et al. 2015). As COs have relativistic behaviours, they can reveal regimes of physics that can not be tested elsewhere. Finally, the evolution of the temperature of NSs with time can constrain their equation of state, one of the most important opened questions in astrophysics (see Yakovlev & Pethick 2004 for a review on cooling NSs).

1.4 Project objectives and thesis outline

As stated in Section 1.2 and Section 1.3, serendipitously detected X-ray sources could help making breakthroughs in our understanding of COs thanks to the discovery of unique and rare objects (e.g., tidal disruption events, IMBHs like HLX-1 – Farrell et al. 2009). Also, sampling standard representatives of COs and AGNs will enable the study of their evolution as a function of cosmic time. This population study will then give further insights into the relationships between compact objects with star and galaxy formation. Recently, the *Swift* team produced a catalog of serendipitous X-ray sources (Evans et al. 2014) detected by the X-ray Telescope (XRT – Burrows et al. 2005). This catalog consists of 151,524 sources over 1905 square degrees, with typical sensitivity of co-added images (covering the same location on the sky) of $\sim 9 \times 10^{-14}$ erg cm^{-2} s^{-1} (0.3 – 10 keV), providing an excellent opportunity for locating new CO candidates. Although the catalog is a factor ~ 1.5 less sensitive than, for example, the 3XMM-DR4[2] catalog, it has a sky coverage nearly 2.5 times larger, placing it between the deep-and-narrow surveys such as the 3XMM-DR4 (Watson et al. 2009) and Chandra BMW catalogs (Romano et al. 2008) and the shallow-and-wide

[2]http://xmmssc-www.star.le.ac.uk/Catalogue/xcat_public_3XMM-DR4.html

surveys, such as the Rosat All-Sky Survey (Voges et al. 1999). The main goal of my master thesis is to propose a classification scheme that will enable to identify the nature of the X-ray sources within the *Swift*-XRT catalog, with particular interest for COs. Once this work is done, dedicated studies of different subgroups of objects and events (such as ULXs or TDEs) will be performed. But this is out of the scope of the present work.

In order to elaborate the selection criteria, I considered a sub-sample of sources from the *Swift*-XRT point source catalog with best quality detection flags and cross-correlated it with 16 external multi-wavelength catalogs providing source type identification. To do so, I used the software TOPCAT (Taylor, 2005) that enabled me to manipulate large databases and helped me visualize different parameters of the *Swift*-XRT catalog in order to search for matches. While the search focuses on finding COs and AGNs, in order to study their properties, cross-match with ordinary galaxies and galaxy clusters catalogs was also done, as well as the cross-match with extragalactic SNR catalogs, because they can often be mistaken for ULXs. Stars can also emit in X-rays, especially the ones with an active corona. This cross-correlation work enabled me to build a golden sample of known type objects (AGN, stars & COs – the most frequent X-ray sources found in X-rays) in order to study their averaged properties. Properties that were taken under consideration are X-ray variability, X-ray to optical/IR flux ratios, X-ray spectral shapes and the spatial distribution along the Galactic latitude. From this analysis work, I derived the selection criteria. They were then applied back to the golden sample for a sanity check and to evaluate the reliability of the classification method. Once this was done, I applied the selection criteria to the rest of the *Swift*-XRT catalog. The average properties of the object group were then studied and compared to the properties found for the golden sample.

In Section 2.1 are described the characteristics of the X-ray telescope and the main scientific objectives of the *Swift* mission, while a description of the main features of the *Swift*-XRT point source catalog is given in Section 2.2. Chapter 3 explains the methodology used for cross-correlating the sources within the *Swift*-XRT catalog with external catalogs to produce the golden

sample and the quantities used for building various science products. The procedure that led to the final list of sources with known types (stars, COs and AGN) is explained in Section 4.1, and their averaged properties are reviewed in Section 4.2. Section 4.3 discusses the derived selection criteria, their efficiency and possible caveats. In Section 4.4, I discuss the application of the classification scheme to the whole *Swift*-XRT catalog clean sample and the average properties of the population of AGN, star and CO candidates. Conclusions and perspectives of this study are given in Chapter 5.

2 The *Swift*-XRT catalog

2.1 The *Swift* mission

Swift (Gehrels et al. 2004) is a multi-wavelength observatory, part of the NASA medium explorer (MIDEX) program, launched on a low-Earth orbit on November 20, 2004. Its key scientific objective is the study of gamma-ray bursts (GRBs). This includes determining the nature of their progenitors, how the burst evolves and interacts with their surrounding environment and the possible discovery of new types. GRBs appear as short-lived bursts of gamma-ray radiation randomly distributed over the sky with a random temporal occurrence, with duration ranging from few milliseconds to several minutes (e.g., Balázs et al. 1998; Horváth et al. 2005). Briefly after the start of the burst, they become the brightest source in the observable Universe. GRBs are thought to be related to the catastrophic formation of stellar mass black holes associated with the launch of powerful ultra-relativistic jets moving along the observer line of sight, following the death of some massive star (with mass larger then 10 Solar masses – MacFadyen & Woosley 1998) or the merger of two compact objects, such as two NS, or a NS and a BH (Eicher et al. 1989). Because of their high redshifts, GRBs can be used to study the early Universe.

The rapid respond of the GRB detection system onboard *Swift* enables detailed multiwavelength observations starting shortly after the burst detection (typically within 3 minutes), until it fades away days or weeks later. These short-term observations and long-term multiwavelength follow-ups are achieved thanks to three co-aligned instruments known as the wide-field

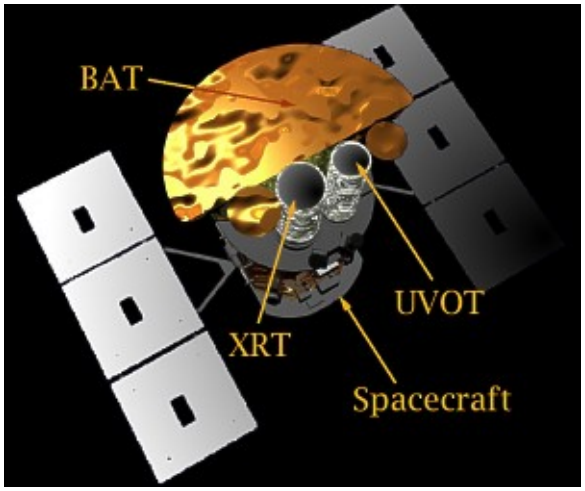

Figure 2.1: The *Swift* spacecraft with its three telescopes: Burst Alert Telescope (15 – 150 keV, FOV 2 sr), X-ray Telescope (0.3 – 10 keV, FOV 23.6"× 23.6") and UV/Optical Telescope (180 – 600 nm, FOV 17"× 17"). Taken from `https://www.swift.psu.edu`.

(two steradians) Burst Alert Telescope (BAT – Barthelmy et al. 2005) and two narrow-field telescopes, X-ray Telescope (XRT – Burrows et al. 2005) and UV/Optical Telescope (UVOT – Roming et al. 2005), as shown in Figure 2.1. The BAT detects the hard X-rays in the 15 – 150 keV energy range, providing the initial position of the GRB within 10 seconds, with an accuracy of about 3 arc minutes[1] at a 90% confidence level. That triggers the rapid autonomous slew of the spacecraft, repointing the two narrow-field instruments towards the GRB position. The XRT refines the GRB position down to a few arc seconds, providing temporal and spectral information of the GRB afterglow. The UVOT further refines the position accuracy down to less then 1" and ensures the follow-up observation of the afterglow, sampling its flux decay in various filters (from UV to optical). The UVOT, unlike the ground based optical telescopes, is not limited by the weather, but only by the presence of bright sources in its field of view (FOV = 17"× 17"). There are six filters from UV to visible (i.e. 180 – 600 nm) making possible the production of spectral emission distribution. The XRT covers

[1] http://swift.gsfc.nasa.gov/about_swift/

the 0.3 – 10 keV energy range, reaching a limiting sensitivity of 2×10^{-14} erg cm^{-2} s^{-1} in 10^4 seconds, with the ability to measure fluxes and spectra over a range covering more than seven orders of magnitude in flux. Its FOV is larger than that of the UVOT (23.6"$\times$ 23.6"). In addition to the GRB core science, *Swift* provides the unique opportunity to perform the first sensitive all-sky survey in hard X-rays. This is one of the *Swift* secondary scientific objectives, and it will help understand the nature of the sources contributing to the cosmic X-ray diffuse background (e.g., Baumgartner et al. 2013).

In addition to the GRB core program, *Swift* performs observations in the frame work of the Guest Investigator (GI) Program and the Target of Opportunity (ToO) Program, both being opened to the whole community. Because of its rapid response in scheduling observations of sources and multi-wavelength capabilities, *Swift* is ideal for the observations of variable sources, such as accreting compact objects (AGNs, XB, ULXs, CVs, etc.), and transient events, for instance TDEs, supernovae and flaring stars. The observations can be carried out over different timescales, depending on the number of revisits (several days to months, even years). Given the sensitivity of the three instruments, in each set of data for a given observed object (a GRB, a GI or ToO target), several objects could be detected in each instrument's FOV. This provides a mine of sources serendipitously detected all over the sky, given the *Swift* GRB observing strategy.

2.2 Main characteristics of the *Swift*-XRT catalog

Because of the *Swift* mission unique features described in Section 2.1, the *Swift*-XRT team produced a serendipitous X-ray source catalog. The *Swift*-XRT Point Source (1SXPS) catalog contains 151,524 X-ray point sources detected by the *Swift*-XRT over 8 years of operation, from which 28,906 are classified as variable (Evans et al. 2014). Two *Swift*-XRT based source catalogs were already released (Puccetti et al. 2011; D'Elia et al. 2013). However, they focused either on the deepest GRB fields or in each observation independently. The 1SXPS catalog took into account both individual observations and deep images. This enabled the detection of fainter sources and added valuable information about source variability. Another advantage

is that pointings are spread over 1905 square degrees on the sky with considerable uniformity (but also with increased density along the Galactic plane), as shown in Figure 2.2. Large sky coverage is of great importance for this work. It enables overlapping of the *Swift* observational areas with the ones from external catalogs, important for the process of source identification. If systematic and statistical errors are combined, the median 90% confidence radial position error of the X-ray sources is 5.5 arc seconds. Analysis of the data was performed in four individual energy bands: in the entire calibrated range of the XRT: 0.3 – 10 keV (total), and in the 0.3 – 1 keV (soft), 1 – 2 keV (medium) and 2 – 10 keV (hard) range.

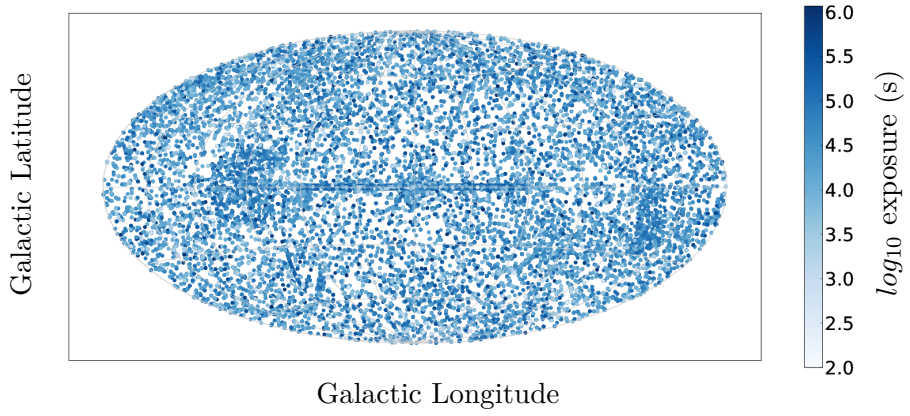

Figure 2.2: The location of the observations within the 1SXPS catalog in Galactic coordinates. Image from Evans et al. (2014). Point sizes do not correspond to the XRT field of view, but their colors indicate the exposure time included in the catalog.

Any observation that overlapped with location that included large-scale diffuse emission was removed (such as the Carina and Crab nebulae, or galactic SNRs), as well as the times from observations when there was increased contamination from light scattered off the sunlit side of the Earth. Indeed, effects caused by the presence of extended sources or optical loading could give rise to spurious detections. To ensure the desired quality of the source sample, a flag was assigned to each image containing artifacts (that could cause such problems) and to each source (Evans et al. 2014). Quality

flag, assigned to sources, indicates a probability that it is a false positive. It is a function of the exposure time and the likelihood value for the source. It can be Good, Reasonable or Poor, where the false positive rate for Good is 0.3%, for Good and Reasonable 1%, and when all the sources from the catalog are included it reaches 10%. In order to avoid, as much as possible, dealing with spurious sources in my work, I used the clean sample from the 1SXPS catalog. It contains all objects qualified as Good and Reasonable, but also those with the catalog column flagged as OK, and those affected only by artifacts, but not in the region covered by them. The clean sample contains 98,762 sources meeting these conditions.

The 1SXPS catalog was cross-correlated with 13 external multi-wavelength catalogs and databases (Evans et al. 2014). If the results from the cross-correlation with the USNO-B1 (Monet et al. 2003) and 2MASS (Skrutskie et al. 2006) catalogs are excluded, 68,638 sources had no external catalog match (33,282 from the clean sample). The exclusion of the two catalogs is due to the high number of spurious matches because of their high sky density and the large median XRT error radius. If they are included, there are in total 20,390 sources in the 1SXPS with no counterparts in any of the 13 catalogs. The 1SXPS catalog does not directly provide identification of the nature of the source, merely a match with previous detections in various wavelengths, except in the case of the SDSS Quasar Catalog, which contains only AGNs and quasars.

Data in the catalog is organized into snapshots and observations, as a result of the *Swift* low Earth orbit, with a period of 96 minutes. This means that a single, continuous on-target exposure can not last more than 2.7 ks. It is referred to as a snapshot, while an observation is a single dataset that consists of several snapshots of a given source made in one day. Snapshots differ in exposure time and the observations differ in the number of snapshots they contain. Both are considered in order to probe source variability on multiple time scales. Snapshot to snapshot variability probes timescales shorter than one day, while observation to observation variability probes long-term timescales. For every source in the 1SXPS catalog, variability estimations on both scales and in each energy band are given.

The catalog also provides two hardness ratios (HR), defined using the count rate measured in the soft, medium and hard bands (see Chapter 3 for details and equations). Observed and unabsorbed flux estimates were also calculated, together with their energy conversion factors (to convert measured count rates to proper fluxes), as well as light curves. When possible, additional spectral information were derived using fixed spectra, interpolation of the HR values and via spectral fitting. Spectral fitting was done for sources with at least 50 net events in the total band, using two spectral models, an absorbed power-law, more suitable for AGNs and COs, and absorbed APEC model (Astrophysical Plasma Emission Code, Smith et al. 2001), more suitable to describe the spectra of stars. This will be explained with more details in Chapter 3. Since it was not possible to do that for all objects, the best spectral property columns are included in the catalog, to make easier the comparison of their features. Spectral information was derived via stacking of all of the data from a given source. It does not take into account possible spectral variation. It can be seen that considerable amount of effort was made by Evans et al. (2014) to transform the raw detector data into related physical quantities, ready for use without much further need for processing required. Thanks to this work, the 1SXPS catalog is extremely useful to investigate the nature of the X-ray sources that it contains.

3 Methodology

In order to divide the 1SXPS sources into various classes and subclasses of objects, selection criteria based on their spatial, temporal and spectral properties had to be established first. To do so, building a sample of known classes of objects from the 1SXPS catalog had to be done. The study of the observed properties for each class will provide a quantitative way to define the needed criteria, consistent with the *Swift*-XRT instrument calibration and sensitivity. A sample of sources from a given identified class of objects is referred to as a golden sample hereafter. I built such a sample by cross-matching the 1SXPS clean sample with specific catalogs providing the classification of a given type of objects. I defined three main categories: compact objects (COs), stars and active galactic nuclei (AGNs). These three classes were chosen because they were identified as the most numerous in the sources detected in X-ray surveys done by other missions (Lin et al. 2012; Watson et al. 2009; Voges et al. 1999). I also performed the search for normal galaxies, galaxy clusters and extragalactic SNRs. The choice of the catalogs used in the cross-correlation scheme was based on completeness, wavelength coverage and the number of objects included in the catalogs. The list of catalogs cross-correlated with the 1SXPS catalog and preliminary matching results are given in Table 3.1.

To perform the cross-correlation of the catalogs and analysis of the data I used the software TOPCAT (Tool for Operating on Catalogs And Tables, Taylor 2005). TOPCAT offers a variety of ways to view and analyze tables, mostly astronomical data, although it can be used for non-astronomical data as well. Input and output formats that are supported with TOPCAT in-

External catalog	One-to-one matches	Multiple matches
Cluster of galaxies in SDSS-III (Wen et al. 2012)	165	0
Stellar-mass black holes in the SDSS (Chisholm et al. 2003)	5	0
IRAS Revised Bright Galaxy Sample (Sanders et al. 2003)	26	0
Radio SNRs in nearby galaxies (Chomiuk et al. 2009)	17	1
Brightness and diameters for extragalactic SNRs (Urosevic et al. 2005)	13	0
SDSS quasar catalog: tenth data release (Paris et al. 2013)	917	0
Catalog of Ultraluminous X-ray sources (Liu et al. 2005)	52	1
General Catalog of Variable Stars (Samus et al. 2007-2013)	689	1
Cataclysmic Binaries. LMXbs. and related objects (Ritter et al. 2014)	208	0
The BAX Database (Blanchard et al. 2004)	8	0
Quasars and Active Galactic Nuclei (13th Ed.) (Véron et al. 2010)	4661	10
Extended Hipparcos Compilation (XHIP) (Anderson et al. 2012)	810	0
Catalog of ROSAT White Dwarfs (Fleming et al. 1996)	2	0
SDSS DR7 white dwarf catalog (Kleinman et al. 2013)	3	0
Isolated neutron stars from Rosat and Swift (Turner et al. 2010)	16	0
LEDA galaxies with DENIS measurements catalog (Paturel et al. 2005)	532	1

Table 3.1: List of the external catalogs of specific types of objects cross-matched with the 1SXPS catalog, together with the number of matches. The second column contains the number of one-to-one correspondence matches with 1SXPS sources, and the third column gives the number of the 1SXPS sources that have multiple matches within that catalog. Positive number of matches does not necessary mean that the main source type of the catalog was found, as most of the catalogs also contain previously incorrect classified objects just to keep track. For instance, all five matches in the stellar-mass black hole catalog are QSO.

clude FITS BINTABLE, ASCII and IPAC (Infrared Processing and Analysis Center) ASCII Column-Aligned format, etc. It offers easy access and search capabilities to the online astronomical databases, such as the Vizier Catalog Service[1], that was used for my work. Apart from the fast access to large volume of datasets, the TOPCAT main capabilities also include viewing and editing tools for the data tables and their column metadata. It offers control over order and appearance of columns or creation of new ones defined by algebraic expression. Being able to define row subsets and to analyze them separately was a particularly helpful element for me in order to isolate the 3 main object groups of interest and build the products (see below). The most used TOPCAT features for my work were the ones that perform matching of rows in the same or in different tables, and concatenating the results to create new ones.

I used two types of matches between the 1SXPS and external catalogs: the Sky and the Sky with Errors algorithm. "Sky" compares the position of two sources on the celestial sphere. So, the required inputs are the Right Ascension and Declination columns, together with the *Max Error* value (maximum permitted separation of matched points around a great circle). The 1SXPS coordinates are in J2000 format, so if that wasn't the case with the external catalog, I applied the needed transformations using the dedicated TOPCAT tools. "Sky with Errors" is similar to the Sky algorithm, but positional uncertainty is given for each row (source) in the input tables, rather than just a single value for the whole catalog. Along with the Right Ascension and Declination columns, an additional *Error* column must also be specified, that gives the error radius corresponding to that position. In the 1SXPS catalog this corresponds to the 90% confidence error radius (the *Err90* column). Among the external catalogs used to perform the cross-correlation, only the Catalog of Cataclysmic binaries, Low-mass X-ray Binaries and Related Objects (7^{th} Edition, Ritter & Kolb 2014, CbXb hereafter) provided such values. In other cases, a constant value for the astrometric accuracy was used as an input. If the standard positional accuracy was not provided, I chose the Sky algorithm, using the median 90%

[1] http://vizier.u-strasbg.fr/

confidence radial position error of the 1SXPS sources (5.5 arc seconds) as an input value. Output results consisted of all the external catalog sources that met these conditions (*All Matches* option in TOPCAT), together with their corresponding 1SXPS counterparts. In five catalogs, double matches appeared in the results, for which two external sources were paired to the same 1SXPS one, as showed in Table 3.1. When the match is performed, TOPCAT calculates the separation in arc seconds between the XRT source and the possible counterpart. The pairs for which this distance was greater than the 1SXPS *Err90* value (of the corresponding individual sources involved in pairs) were flagged. Number of found matches for each catalog is given in Table 3.1. I note that the median 90% confidence radial position error of the 1SXPS catalog was used only when the initial match between catalogs was performed, while in the cases of flagging process and further checks of the produced pairs, the 90% confidence radial position error associated with each 1SXPS source separately was the one considered. Before the matching process itself, I made various types of cleanings on the external catalogs when needed, in order to improve the quality of the final result. It usually included discarding the sources with bad astrometry, the ones that contained superimposed objects (in the catalogs that provided such flags), or the ones for which no type classification was given.

X-ray sources are divided into one of the three previously mentioned classes: AGNs, stars and COs. There are also SNR, galaxy and galaxy clusters, but for these latter groups property analysis will be done in a second time (see Chapter 5). The classification of AGN in sub-classes was based on the catalog of quasars and active nuclei by Véron-Cetty & Véron, 13^{th} edition (2010, VV13 hereafter). The subclasses are: quasars (QSOs), AGNs (without further classification), BLLac objects (BLLac), liners (Lin), Seyfert 1 (Sy1), Seyfert 2 (Sy2) and narrow-line Seyfert 1 (NlSy1), similar as what was done in Lin et al. (2012). I also adopted the same scheme in the case of Seyfert galaxies with broad polarized Balmer or Paschen lines, including them in the group of Seyfert 2 galaxies. Lin et al. (2012) note that they are generally simply classified as Seyfert 2 galaxies in SIMBAD[2]

[2]http://simbad.u-strasbg.fr/simbad/

(the Set of Identifications, Measurements, and Bibliography for Astronomical Data). For stars, the subclasses are: Orion-variables (OrV), flaring and eruptive stars (FlE), pre-main-sequence stars (PrS), variable stars (Vr), including the types that were classified in the General Catalog of Variable Stars (GCVS, Version 2013, Samus et al. 2009) as rotating, pulsating or eclipsing variables, and finally stars (St) that are mostly Main Sequence ones. Compact objects were divided into cataclysmic variables (CV), white dwarfs (WD), X-ray binaries (XB) and ultra-luminous X-ray sources (ULX).

Matches between the results from different catalogs were performed. The purpose was to search for X-ray sources that were found in several external catalogs. As a result, groups of the same 1SXPS source and different external catalog sources were formed. For instance, if an AGN or a galaxy appear in one of the two cluster catalogs, a flag of cluster membership was assigned to it. I made further checks of these groups of sources, to see whether the classes or subclasses of objects contradict each other. If so, these groups are then placed in a separate row subset within the resulting table. Not all type and subtype mismatches were considered as a problem. For example, if an object was defined as a QSO in the SDSS quasar catalog: 10^{th} data release (Paris et al. 2013), but as a Sy1 galaxy in VV13, the VV13 identification was prefered. Likewise, the two general galaxy catalogs, the LEDA (Lyon-Meudon Extragalactic Database) galaxy catalog with DENIS (DEep Near Infrared Survey) measurements (Paturel et al. 2005) and the IRAS (InfraRed Astronomical Satellite) revised bright galaxy sample (Sanders et al. 2003) contain both normal galaxies and AGNs. Because of that, some 1SXPS sources classified as AGNs are expected to have a counterpart in these catalogs also. In general, if one catalog provided a subclass that was different, but not contrary to the one from the other catalog, the source classification was considered valid. Consequently, if a source was classified as Orion variable in one catalog, and pre-main-sequence Orion variable type star in another, the OrV designation was assigned to it. Also, if the star belongs to the group of eruptive stars (for the classification given in GCVS) but was refered in extended Hipparcos compilation (Anderson et al. 2012, HIP hereafter) to by just a variability symbol (V*), the star was considered as an

eruptive one. This was mostly due to the difference in designation system between GCVS and HIP (HIP uses the one from SIMBAD). In some cases, one counterpart in the group (of the same 1SXPS object found in multiple catalogs) was located outside the *Swift* 90% confidence level error radius of the 1SXPS source in question. Then the separation of matched objects from different catalogs was calculated. If it was bigger than the corresponding 1SXPS radial error of the X-ray source, the match was flagged as possibly spurious (Figure 3.1). Once golden sample was judged of sufficiently good quality, I studied the sample properties.

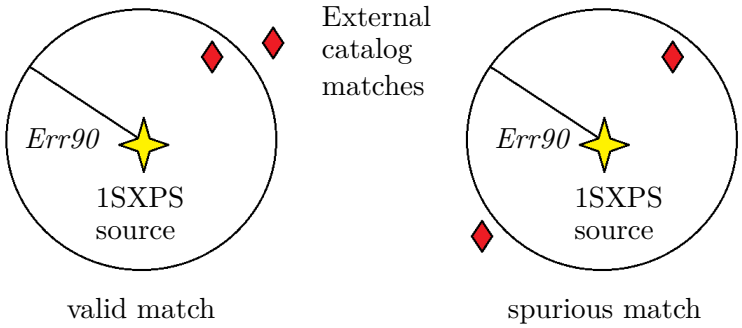

Figure 3.1: Example of a valid and a spurious match when the 1SXPS source is found in multiple external catalogs, with one source lying outside the 1SXPS 90% confidence error radius (*Err90*). Match is considered as spurious if the separation of two external catalog sources (red diamonds) is greater than the Err90 radius of a 1SXPS source (yellow star).

To investigate the general properties of a given classes of objects, I consider the following quantities:

- the Galactic longitude and latitude to study the spatial distribution of the X-ray sources;
- two hardness ratios HR1 and HR2;
- the probability that the source is constant from snapshot to snapshot and from observation to observation in different energy bands;
- the power-law photon index Γ_{PL} and the APEC temperature distribution;

- the mean observed source flux in the total band (0.3-10 keV); and
- the IR and optical fluxes when available.

All the above quantities beside the optical and IR fluxes are already provided in the 1SXPS catalog.

The two hardness ratios are defined in the catalog as follows:

$$HR1 = (M - S)/(M + S) \tag{3.1}$$

$$HR2 = (H - M)/(H + M) \tag{3.2}$$

where S, M, H refer to the soft (0.3 – 1 keV), medium (1 – 2 keV) and hard (2 – 10 keV) band background-subtracted count rates, respectively. They provide an approximate measure of the source spectral shape (i.e. the distribution of counts versus energy), and are going to be used to build color-color diagrams for every class of objects separately. The two HR values are then plotted as a data point on the color-color diagram. From the location of a source in the color-color diagram, it can be concluded if the source has a soft or hard spectrum (most counts being at low or high energy, respectively), or if the source is absorbed (see Chapter 4).

The variability properties can provide important clues about the source type. Indeed, the AGNs and COs are known to display variability on various timescales. AGN emission can change appreciably on time scales ranging form hours to days, even weeks and months, while COs can be variable on even shorter timescales. The variability amplitude is also larger in COs when compared to AGNs and stars (e.g., Lin et al. 2012). Some stars are also known to be variable or flaring in X-rays (Carroll & Ostlie 2007). The 1SXPS catalog gives the probability for the null hypothesis that the source is constant from observation-to-observation and from snapshot-to-snapshot, in all of the four energy bands. In this way, variability can be probed on multiple timescales and for the soft and hard part of the X-ray emission. A measurement of how well a given null hypothesis is compatible with the observed data, without specific reference to any alternative hypothesis, provides a goodness-of-fit test. It can be done by constructing a test statistic whose value itself reflects the level of agreement between the observed mea-

surements and the ones predicted by the null hypothesis. To determine the probability that the source was variable (or the probability that the null hypothesis of the X-ray source being constant is false), Evans et al. (2014) used Pearson's χ^2 (Pearson 1900) statistic, given by equation (3.3).

$$\chi^2 = \sum_{i=1}^{N} \frac{(n_i - \nu_i)^2}{\nu_i} \tag{3.3}$$

χ^2 statistic then gives the quadratic sum of deviations between observed (n_i) and expected (ν_i) values, measured in units of the corresponding standard deviations. Applied to the light curves, n_i is the data and ν_i is a constant source flux model in bin i. The P-value or the significance level is therefore given by the integral of the χ^2 distribution from the observed χ^2 to infinity. For the details see Evans et al. (2014). Note that there is no information on how strong variability has to be before it is detected. This is a function of variability type, exposure, source brightness, and many other factors, so it can be determined only on per-source basis.

Evans et al. (2014) also extracted spectra for sources showing more than 50 net counts. The spectra were then fitted using two basic models: an absorbed power-law (PL) and an absorbed APEC (Smith et al. 2001) spectrum (using fixed spectra, interpolation of the HR values or fitted spectra). The power-law (PL) photon index (Γ_{PL}) measures the dependence of the photon flux (S) on energy (E) as follows $S \propto E^{-\Gamma}$, and its value depends on the processes producing the radiation. The APEC code predicts spectra (see Smith et al. 2001) for collisionally ionized plasma (line and continuum). These predicted fluxes may in turn be compared with an observed spectrum. It is temperature dependent, so that the plasma temperature (kT) can be extracted. I used the Γ_{PL} and kT values derived by direct spectral fitting, but only those for which the reduced χ^2-values, that serves as indicator of the goodness of the fit, are between 0.6 and 1.5, in order to get the true behavior of the three object groups. Therefore, poor fits were discarded.

Mean observed fluxes (in erg cm^{-2} s^{-1}) were taken from the best spectral property column. The methods to derive the flux can actually differ from source to source. Mean observed fluxes were used to compute the X-ray to

optical and IR flux ratios. The optical fluxes were obtained by performing a cross-match with the USNO B1.0 (Monet et al. 2003) catalog, while the IR fluxes were derived using the 2MASS catalog (Skrutskie et al. 2006). I used the $R2$ magnitude from the USNO B1.0 catalog to calculate the optical flux, or $R1$ when $R2$ was not available (6% of the cases), while for the IR flux the 2MASS K_S magnitude was used. The conversion from magnitudes to fluxes (in erg cm^{-2} s^{-1}) was done using equation (3.4) and equation (3.5)

$$\log(F_{OP}) = -R2/2.5 - 5.37 \tag{3.4}$$

$$\log(F_{IR}) = -K_S/2.5 - 6.95 \tag{3.5}$$

following Maccacaro et al. (1988) for optical and Cohen et al. (2003) for IR fluxes, in a similar way as done in Lin et al. (2012). Because the size of the two catalogs was too big to be downloaded, the cross-match was not performed using TOPCAT, but instead the VizieR X-Match service[3]. The median 90% confidence radial position error of the 1SXPS sources, 5.5 arc seconds, served as an input for the permitted separation for both catalogs. The results were then checked in order to find the counterparts that lay outside the *Swift* 90% confidence level error radius of the 1SXPS source in question (the *Err90* column). Such results were discarted.

Before applying the criteria based on the properties described above to the non-identified sources of the 1SXPS clean sample, I applied these criteria to the golden sample in order to check what percentage of each class of objects would be correctly retrieved, and also to understand why the new type classification differs from the previous one. As a result, the golden sample sources were reclassified again as AGNs, COs or stars. The discrepancies observed between the classification obtained using external catalog cross-match and the one when using selection criteria are discussed in the following chapter. This sanity check is essential to test the reliability of the method. When this was done, the same method was applied to the rest of the 1SXPS catalog clean sample. I note that this strategy was applied with success for classifying a sub-sample of bright *XMM-Newton* sources by Lin et al. (2012) using the 2XMMi-DR3 catalog (Watson et al 2009).

[3]http://cdsxmatch.u-strasbg.fr/xmatch

4 | Results

4.1 Building the golden sample

To lower the uncertainties in the results, and to get more accurate group properties, I proceeded with the following actions before constructing the products. First, all the 1SXPS sources that had multiple matches within one of the external catalogs were removed from the matched source list. Their number by catalog is given in the third column in Table 3.1. Although the "All Matches" option was used while searching for counterparts, only a small number of the 1SXPS sources (14 in total) had multiple objects assigned to them. This can be seen as an indicator of a good source association. Next, all the 1SXPS sources that had counterparts in more than one catalog, but with conflicting classification, were also removed into a separate table. In total there are 38 such objects, mostly classified as CV in CbXb (20 of them) but as XB in GCVS. CVs are a subtype of XBs, but both of the catalogs have an additional or completely separate label in the case of CVs, differentiating them in that way from the XBs with NS or a BH as the primary star. I chose to follow that designation system in my work. There are also 8 ULXs that were found as AGNs or SNRs. This is consistent with the remark in the paper of the catalog of ultra-luminous X-ray sources (Liu & Mirabel 2005), in which the reader has been warned about possible misclassification with SNRs or background AGNs. I note that 658 sources in the 1SXPS catalog had matches in more than one catalog, and only 38 of them had counterparts with a conflicting type. This also indicates the good association between matched sources, but, for these data to have a certain weight, more analysis should be done. Finally, using the median

90% confidence level radius value as input for the cross-match resulted in external catalog conterpart being outside the *Err90* radius for some of the 1SXPS sources. These matches were considered spurious and were removed from the results. There are in total 579 such objects. Exception was made if the considered 1SXPS source had a second, valid match in another catalog, with the distance between two external catalog counterparts smaller than the provided 90% confidence radius (Figure 3.1).

The remaining sources are considered as a sample of desired cleanness (golden sample), and were used to study the properties of the AGNs, COs and stars. The golden sample contains 6798 sources, from which 14 AGNs and galaxies were also found as galaxy clusters and 618 of sources had a match in 2 or more external catalogs. Most sources are AGNs (4929), corresponding to 73% of the golden sample. The rest consists of 361 galaxies, 17 SNRs (or their knots), 1125 stars and 233 COs.

Similar procedure was done regarding the 2MASS and USNO B1.0 catalogs in the search for optical and IR counterparts. When considering only the one-to-one 1SXPS - USNO B1.0/2MASS corresponding matches that lie inside the 90% confidence radial position error, 91% of the golden sample has optical counterpart while 53% has IR counterpart, but these percentages get lower when the whole 1SXPS clean sample is considered. Optical counterpart was found for 44% of sources in the 1SXPS clean sample while the IR counterpart for 20%. The optical/IR counterpart coverage gives a sense of the efficiency of the optical/IR based selection rule that will be discussed in the forthcoming section. It is also important to keep in mind that all sources in the 1SXPS catalog do not necessarily have all their spectral properties calculated. More detailed statistics for subclasses and other main groups, including the optical/IR coverage, is given in Table 4.1.

Subclasses	Number	Classes	Number(%)	Optical	IR
QSO	2907	AGN	4929 (73%)	90%	42%
AGN(rest)	311	Stars	1125 (17%)	94%	93%
BL Lac	327	CO	233 (3%)	73%	49%
Liners	40	Galaxy	361 (5%)	94%	84%
Sy1	932	Galaxy clusters	133 (2%)	86%	59%
NlSy1	161				
Sy2	251	SNR	17 (0.3%)	24%	6%
OrV	155				
FlE	72				
PrS	10				
Vr	230				
St	658				
WD	4				
CV	150				
XB	47				
ULX	32				

Table 4.1: Number of objects in the golden sample, divided into their type classification (main type: AGN, stars and COs and subclasses for each type). Fourth column gives the number of sources for each class of objects in the golden sample. The numbers quoted for galaxies and galaxy clusters correspond to the number of sources for which there is no match with the AGN class and no match with the AGN and galaxy classes, respectively. In parentheses, I provide the ratio of the number of sources of a given type over the total number of sources in the golden sample. The fifth and sixth column contain the percentage of AGNs, COs and stars which have calculated optical and IR fluxes.

4.2 Investigation of the properties of the golden sample

4.2.1 Spatial distribution

The properties of each source group (built with quantities described in Section 4.1) from the golden sample are discussed here, starting with spatial distribution of each source group. Figure 4.1 shows the distribution of AGNs, stars and COs with respect to the Galactic latitude b. Spatial distribution in both Galactic coordinates is not shown because the over density of sources causes overlapping of points and, consequently, the true number of sources can not be seen. AGNs concentrate at high Galactic latitudes, with an excess in the northern Galactic hemisphere. This asymmetry can be explained by the fact that the AGN catalogs used for the cross-correlation, the VV13 (Véron et al. 2010) and SDSS quasar (Paris et al. 2013) catalogs, were based on observations primarily performed in the northern hemisphere. Similar results were obtained by Lin et al. (2012) when classifying a subsample of the 2XMM sources. Only 5% of AGNs lie within the area of $|b| < 15°$. This is due to the large absorption along the Galactic plane. Also, galaxy surveys often avoid this area for the same reason, therefore focusing at higher latitudes.

Stars concentrate at the low Galactic latitudes. Note the peak in the star distribution close to $b = -20°$ that corresponds to the location of the Orion Nebula, a high star-forming region. About 28% of the stars are within $|b| < 10°$, and 53% within $|b| < 20°$, consistent with the fact that most of the stars are typically in the Galactic plane. Stars at high latitudes are the ones closest to us.

For COs, the highest density is also in the low latitude region, where 38% are within $|b| < 10°$, and 50% within $|b| < 20°$. COs outside that interval correspond mostly to extragalactic sources, such as ULXs.

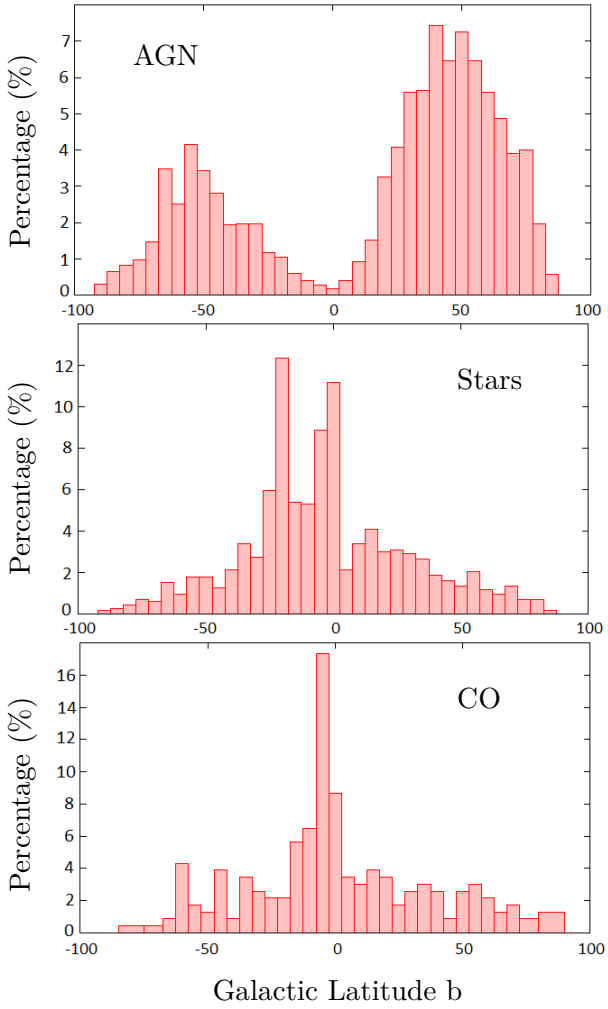

Figure 4.1: Distribution of sources from the golden sample of AGN, star and CO groups as a function of the Galactic latitude. Note that the bin sizes do not correspond to equal spatial area.

4.2.2 Spectral properties

Figure 4.2 (left) shows the density distribution in the X-ray color-color diagram showing the relationship between the two hardness ratios (see Chapter 3). The overplotted dashed squares enclose 50% of the data points. For AGNs, most of the sources are concentrated in the center of the diagram. This is consistent with the remark made by Evans et al. (2014), stating that

the three partial bands in the 1SXPS catalog (soft, medium and hard) have an energy range that would give an approximately similar number of events in each of the three spectral bands for a typical AGN spectrum. The region of two groups of AGNs (not visible in color because of the low point density) is also marked on the diagram (full lines). The first one (the ellipse) is the Sy2 group, corresponding to the top horizontal branch with HR2 between 0.8 and 1.0. Sy2 galaxies in the AGN classification scheme are expected to be observed through a dusty torus masking continuum radiation coming from the central engine (see Section 1.1). This could lead to high absorption column density resulting in a deficit of soft photons (HR1 > 0). Sy2 galaxies in some cases also display soft excess that lead to HR1 values < 0 (see Section 1.1). This accounts for the top horizontal branch in the color-color diagram. Similar distributions were obtained by Lin et al. (2012). The second group consists of NlSy1 outliers in the high left-upper part of the diagram, that are isolated as a separate group from the rest of the NlSy1 that occupy the lower-mid part of the diagram (in the area of the highest AGN density). Examination of the spectra shows a small number of counts in the medium band, with higher number of counts in the hard band, coming from a possible contamination by the instrumental background, or in some cases from the presence of a strong iron line (at about 6 keV, depending on the redshift) associated to the source, giving rise to large HR2 values (see equation (3.2)). Example of such spectrum for one of the NlSy1 outliers is given in Figure 4.3 (Evans et al. 2009).

The density distribution for stars is puzzling. Figure 4.4 shows locations of the kT-values in the HR1-HR2 space from an absorbed APEC model, appropriate for describing the X-ray emission from stars (Raymond 2005). Comparing the distribution found for stars with the one in Figure 4.4, we see that most of the observed distribution does not occupy the parameter space on the color-color diagram that corresponds to any of the kT temperatures derived from the APEC model. The stars in the left vertical branch on the color-color diagram (green dashed square) represent 21% of the total number of stars considered here. Only about 10% of the stars in total have calculated kT temperatures with reasonably good fits, and the values are

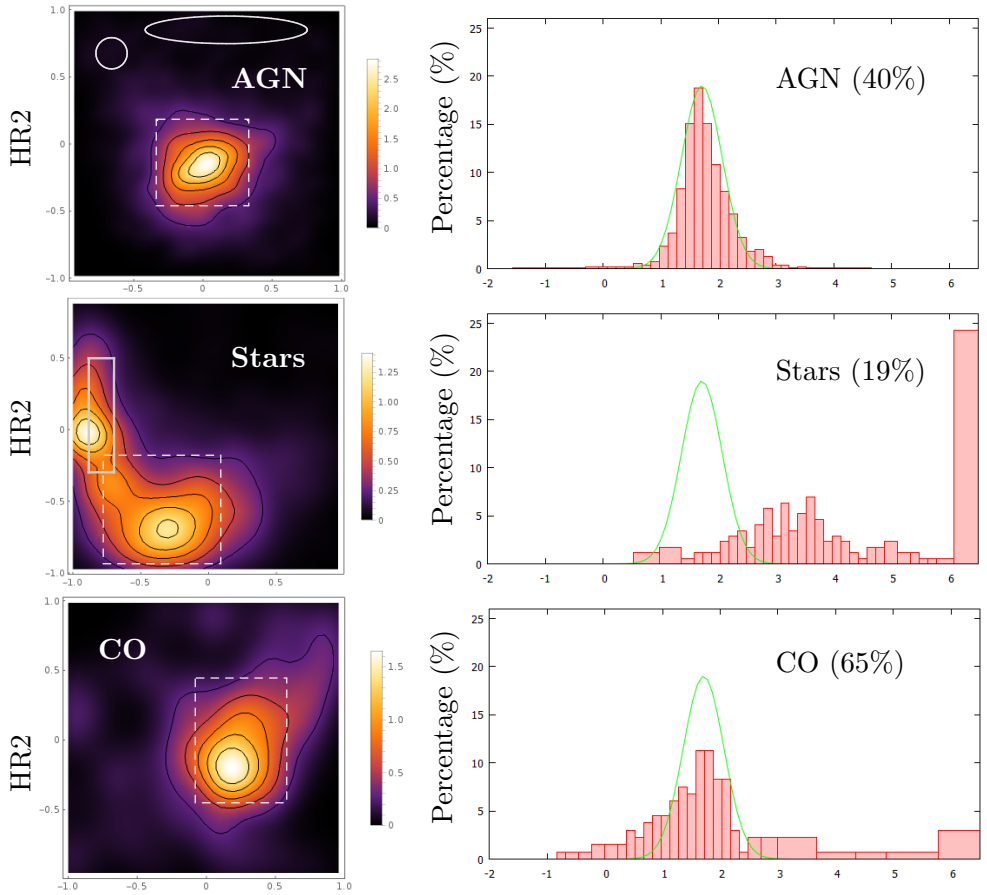

Figure 4.2: Left - X-ray color-color diagrams for the golden sample of AGNs, stars and COs. Because of the large number of sources, the color-color diagrams show the source density distribution in arbitrary units. Dashed and full-line contours are plotted for reference. For the number or characteristics of objects they enclose, see Section 4.2.2. Right - Distribution of the power-law photon index (Γ_{PL}) for the same source candidates. A normal distribution with a mean of 1.71 and a standard deviation of 0.35 is also plotted in each of the right panels for reference. The Γ_{PL}-values greater than 6.0 are placed into one bin. In parentheses, I provide the percentage of AGN, star and CO candidates for which the Γ_{PL}-values are available.

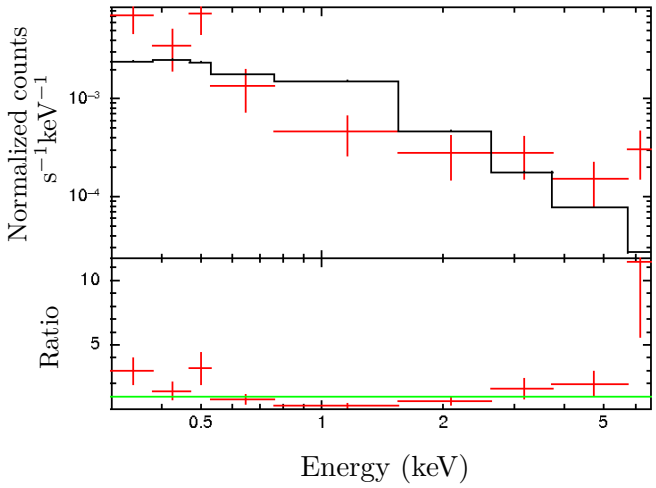

Figure 4.3: The *Swift*-XRT time averaged spectrum of a NlSy (1SXPS J135542.5 +644045). The solid line corresponds to the best-fit power-law model. Image retrieved from the *Swift*-XRT data products generator.

in this case in a physically reasonable range, as shown in Figure 4.5. These stars occupy mostly the lower half of the area enclosed by the overplotted dashed square. This corresponds to the prediction of the APEC model. The leftovers do neither have calculated kT-values at all or the spectral fitting results using an absorbed APEC model are poor. I made several checks, including the recalculation of the hardness ratios using the count rates provided in the 1SXPS catalog, together with the equations (3.1) and (3.2). No inconsistencies were found. Stars rarely show hard X-ray spectra, except for Be stars (Lopes de Oliviera et al. 2007) that can be very hard, or in case of X-ray flares for coronally active stars (Lin et al. 2012). This is not the case for the subclasses that form the tail in the upper part of the diagram, as they are in majority Vr and St stars. This problem will be further addressed when discussing the PL photon index distribution.

The location of the CO group on the color-color diagram with respect to the AGNs is consistent with the work done by Lin et al. (2012) on the *XMM-Newton* sources. The curved spreading that corresponds to sources with lower Γ_{PL}-values (i.e. harder spectra – see Figure 4.6), can also be seen in the CO case. This is in agreement with their large spread in the

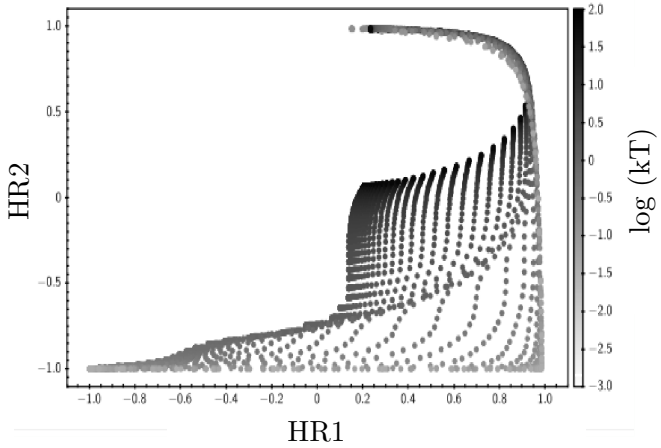

Figure 4.4: Locations of the temperature values from an absorbed APEC model in the color-color space. Each point also has the Galactic absorption column density (N_H) value not shown here. Image from Evans et al. (2014).

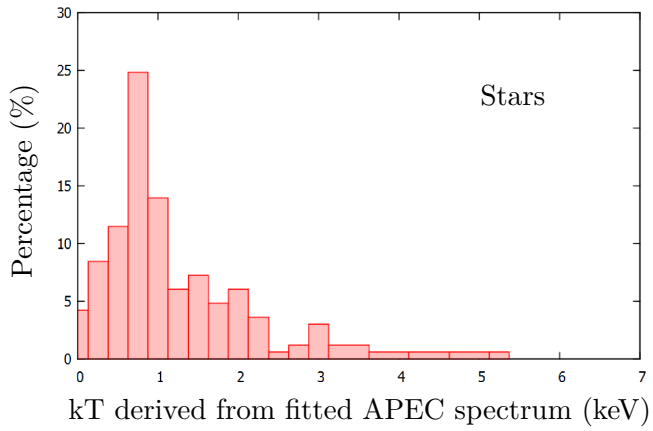

Figure 4.5: Distribution of the APEC temperature, derived through direct spectral fitting, for the class of stars from the golden sample. Temperature values considered are the ones with reduced χ^2 between 0.6 and 1.5.

PL photon index (Γ_{PL}) distribution that extends to lower values (down to -1) – see Figure 4.2 (right). The spread is likely to be due to spectral state transitions (see Section 1) known to display different spectral shapes. Similar values are reported in the literature. Feng & Soria (2011) note that

a broad distribution of photon index values for ULXs without clear gaps indicate that two regimes of accretion are smoothly connected, peaking at $\Gamma_{PL} = 1.8 - 2.0$ with harder ($\Gamma_{PL} < 1$) and softer ($\Gamma_{PL} > 3$) components. Further, Remillard & McClintock (2006) note that for BHBs, the "very high" state is often characterized by $\Gamma_{PL} > 2.5$, while low/hard state with $\Gamma_{PL} < 1.7$. The very large Γ_{PL}-values ($\Gamma_{PL} > 4$) are not physical. This instead indicates a very soft spectrum that likely corresponds to sources being in the high-soft or "thermal" state (Remillard & McClintock 2006). NS-XRBs could also display soft spectra and therefore very steep Γ_{PL} when only the emission from the NS surface is seen (see Tanaka (2000) for overview on observational differences between NS-XRB and BH-XRB). In Figure 4.7, spectra of two XBs (Evans et al. 2009) with high and low Γ_{PL}-value are given as an example, where it can be seen that high Γ_{PL}-values correspond to soft and low Γ_{PL}-values to hard spectra. The Γ_{PL} distribution for AGNs peaks in the same range as for COs. The distribution shows the shape of a normal distribution with an average value around 1.71, consistent with typical values derived for AGNs (e.g., Corral et al. 2011 – see Section 1.1) and with the result obtained by Lin et al. (2012) on the sample of AGNs observed by *XMM-Newton*. They found an average value of $\Gamma_{PL} = 1.9$ with the same shape for the distribution.

Stars show much softer spectra and more spread distribution with $\Gamma_{PL} > 2$. Variable stars (Vr) and stars without further classification (St) make 91% of the stars with $\Gamma_{PL} > 5$. For lower Γ_{PL}-values, around half of these stars are Orion-variables (OrV) and eruptive and flaring (FlE) stars (spreading in the bottom right part of the color-color diagram with HR1>0.0), suggesting that the majority of detections with low Γ_{PL}-values are due to stellar flares. It should be noted that only about 15% percent of the stars has calculated reliable Γ_{PL}-values, and the most of them lie in the lower half of the full-lined square plotted over a HR1-HR2 diagram in Figure 4.2. This could suggest that the rest of the stars are in fact other types of objects, but there are two problems with this suggestion. First, in this case number of stars will be too small compared with other object types, as previous sensitive X-ray surveys showed that stars are numerous in X-rays. Second,

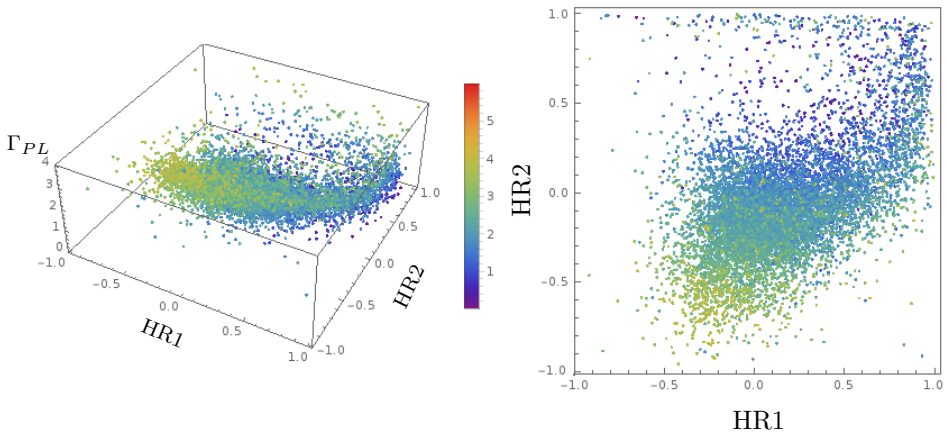

Figure 4.6: Γ_{PL}-values for the golden sample, with χ^2 between 0.6 and 1.5, shown in color-color space. The lowest Γ_{PL}-values are represented with blue color and the highest values with red, as shown in the color legend in the middle of the figure.

stars with optical and IR counterparts occupy the plotted distribution in the HR1-HR2 diagram as a whole, including the hard upper part of the moon-like shape. Yet, the distribution of the X-ray to optical/IR flux ratio of that sample is separated from the AGNs and COs, as seen in Figure 4.8. Also, PL should not provide a good fit for stars in general. The APEC model is a better one to represent emission from stars. High Γ_{PL}-values for stars do imply that the PL model is not physical and thermal emission is more likely. Spectra that were extracted for some of these sources show in general a very soft source with low photon count in the medium or hard energy band. One likely possibility is that because their spectra are soft with almost no counts in the medium and hard bands, additional counts in the hard band due to the instrumental background would give rise to high value of HR2, similar to the case of some NlSy1 galaxies. Supporting this claim is the fact that these stars are all fainter sources, where all the brighter ones ($\log(F_X) > -12$) occupy the parameter space that corresponds to the kT temperatures derived from the APEC model. Since the origin of the discussed moon-like shape distribution remains unsure, I did not use the HR1-HR2 diagram of stars when deriving the selection criteria for this type

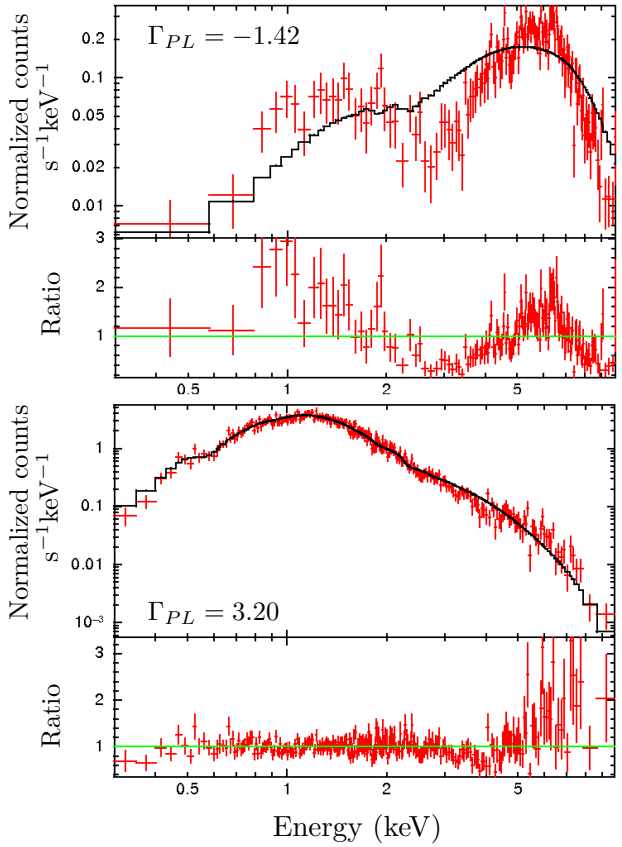

Figure 4.7: The *Swift*-XRT time averaged spectra of two XBs. Top - 1SXPS J090206.7 -403318 with low photon index ($\Gamma_{PL} = -1.42$). Bottom - 1SXPS J191022.7 -054757 source with high photon index ($\Gamma_{PL} = 3.20$). Image retrieved from the *Swift*-XRT data products generator.

of objects.

Figure 4.8 shows that the star, AGN and CO distribution is consistent with the expectation that stars radiate less in X-rays than in optical/IR, while it is the other way around for COs and AGNs. I note that Lin et al. (2012) obtained similar distributions. The vertical line in Figure 4.8 shows the cutoff in the distribution for stars with respect to AGNs and COs. The two peaks seen in the star distribution contain different types of stars. For example, 88% of stars with $-5 < \log(F_X/F_O) < -4$ are main sequence ones (designated as St, stars without further classification), while Orion-variables (OrV), eruptive and flaring stars (FlE) make more than 50% of sources with

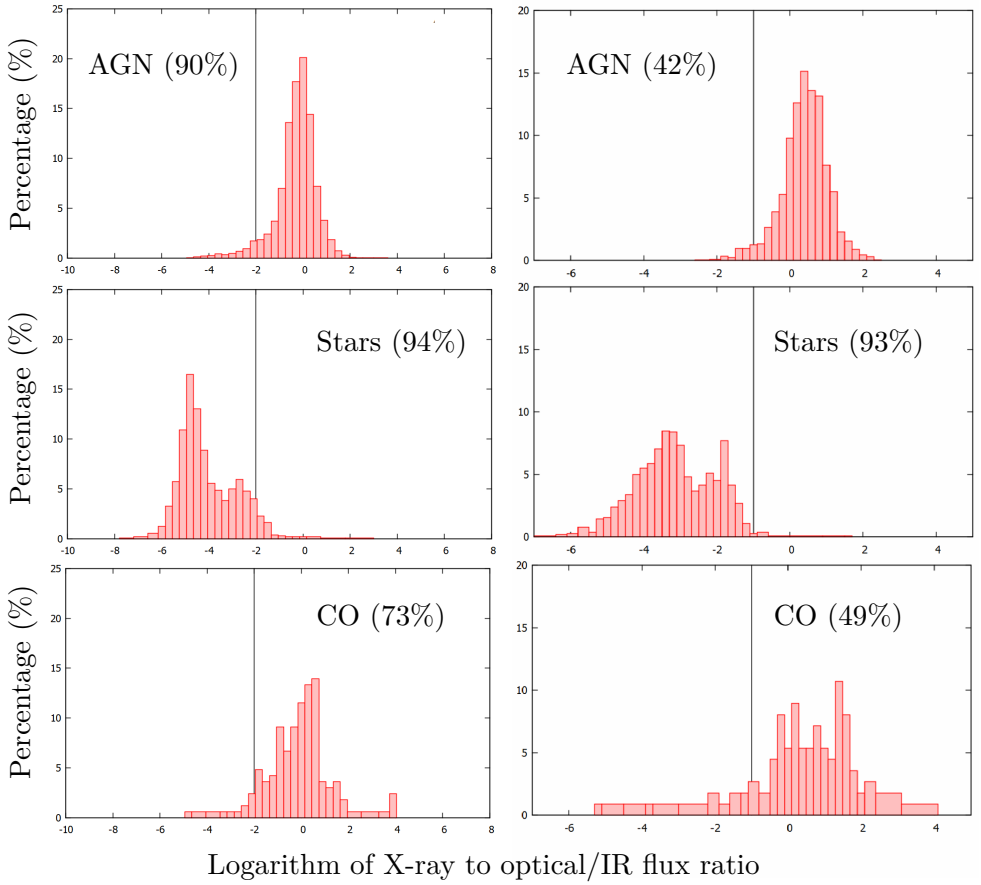

Figure 4.8: Left - Distribution of the X-ray to optical flux ratio for the golden sample of AGNs, stars and COs. The vertical solid line makes an arbitrary separation between stars and AGNs-COs. The optical fluxes were derived from the USNO B1.0 $R2$ or $R1$ magnitude. Right - Distribution of the X-ray-to-infrared flux ratio for the same three groups. The vertical solid line makes an arbitrary separation between stars and AGNs-COs. The infrared fluxes were derived from the 2MASS K_S magnitude.

$-3 < \log(\mathrm{F_X}/\mathrm{F_O}) < -2$, with almost all of the other half of stars being designated as variable ones (Vr). Similar percentages of these subclasses were found in the two peaks seen in $\log(\mathrm{F_X}/\mathrm{F_{IR}})$ distribution. The percentage of stars that have optical (94%) or IR (93%) counterparts found in comparison to AGNs and COs is also as expected, as these objects radiate at these

wavelengths more than the other two groups (see Table 4.1). Only 42% of AGNs and 49% of COs in the golden sample have IR counterparts, while these values get higher (90% and 73%, respectively) when optical wavelengths are considered. COs, consisting of a number of different types of objects with different regimes of accretion, exhibit a wider distribution. For example, while CV distribution is limited to $-2 < \log(\mathrm{F_X/F_O}) < 2$, XBs can have $\log(\mathrm{F_X/F_O})$ values up to 4.0. Together with the differences seen in the photon index distribution between various classes of objects, $\mathrm{F_X/F_{O/IR}}$ distribution will be used to define selection criteria (see Section 4.3). Given the vertical line in Figure 4.8 has been chosen arbitrarily, some contamination between different classes of objects around the cutoff in optical and IR can be anticipated.

4.2.3 Temporal properties

Figure 4.9 (bottom) shows the probability distribution that the source is constant between observations in the total (0.3 – 10 keV) and hard (2 – 10 keV) energy bands for the three main classes of objects, designated hereafter as $P0_{OBS}$ and $P3_{OBS}$ for the total and hard band, respectively. Similarly on the top is the probability distribution that the source is constant between snapshots, designated hereafter as $P0_{SN}$ for the total band and as $P3_{SN}$ for the hard band. While these probabilities are also provided for the other two bands, I focus on the ones above, since I used them for defining the selection criteria. It can be seen that the COs are the most variable group, with around 50% of objects having the $P0_{SN}$ and $P0_{OBS}$ less than 0.05. This value means that, after evaluation of subsequent observation and snapshot data, there is 5% probability that the source is not variable. AGNs are still variable, but with smoother distribution while stars are the least variable group in hard X-rays.

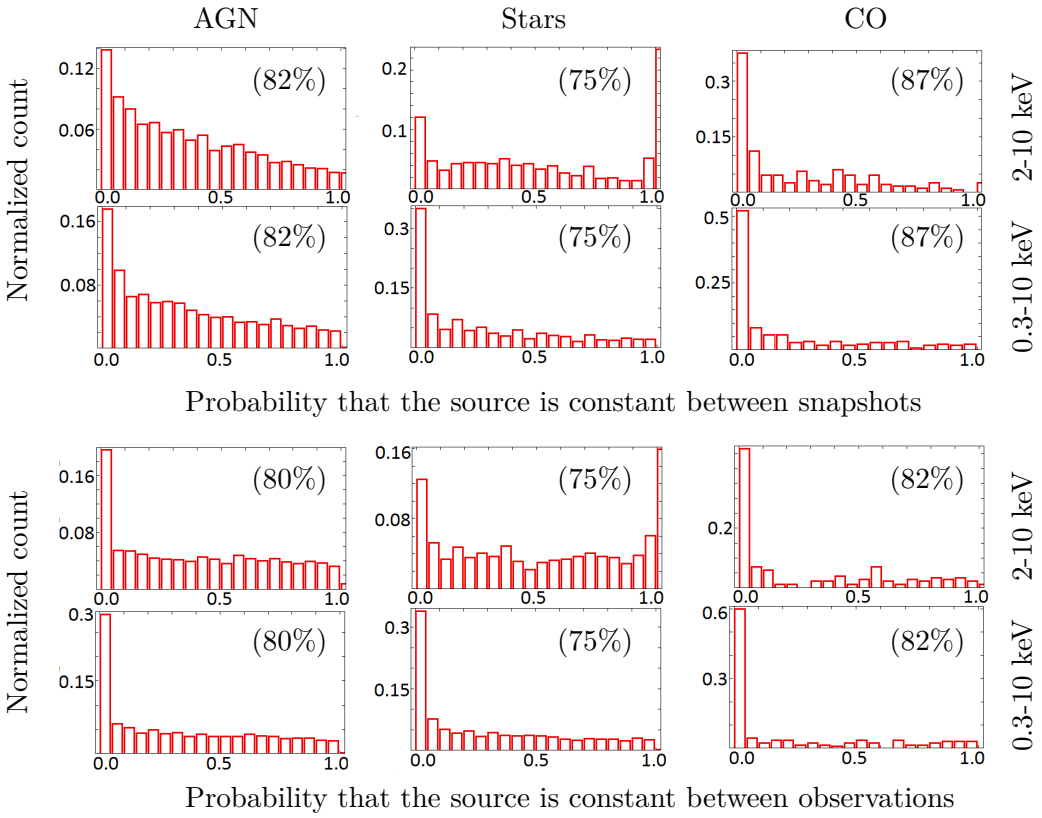

Figure 4.9: Probability that the source is constant from snapshot to snapshot (top panel) and from observation to observation (bottom panel) for the three main golden sample classes of objects in two energy bands: 2 – 10 keV and 0.3 – 10 keV. On the y-axis is shown the normalized number of sources of a given type. In parentheses, I provide the percentage of AGN, star and CO candidates for which the plotted quantities are available.

4.3 Selection criteria

Considering the studied properties of the different classes in the Section 4.2, I was able to define selection criteria to distinguish X-ray sources either as AGNs, stars or COs. Below I describe what are these selection criteria and list them in the order they were applied.

- Sources with PL gamma index $\Gamma_{PL} > 3.0$ and $\log(F_X/F_{OP}) > -2.0$ or $P3_{OBS} < 0.05$ in the hard band are classified as COs.

- The remaining sources with PL gamma index $\Gamma_{PL} > 3.0$ are classified as stars.
- Sources with PL gamma index $\Gamma_{PL} < 1.0$ are classified as COs.
- Sources with $\log(F_X/F_{OP}) < -2.0$ are classified as stars (this will isolate the rest of the stars from the $1.0 < \Gamma_{PL} < 3.0$ interval or from sources for which Γ_{PL} is not calculated).
- Sources with $\log(F_X/F_{OP}) > 2.0$ are classified as COs.
- Sources with $\log(F_X/F_{IR}) < -1.5$ are classified as stars.
- Sources with $\log(F_X/F_{IR}) > 2.5$ are classified as COs.
- Sources with HR1 > 0.0, $P3_{OBS}$ or $P0_{SN}$ values less than 0.05, and their Galactic longitude between $20° < b < 20°$, are classified as COs.
- The remaining sources are assumed to be AGNs.

Looking at the product statistics from the golden sample, this should isolate between 25 – 50% of the COs from that area, and should lead to $< 5\%$ of misclassification of AGNs as COs. A flowchart depicting the selection process is shown in Figure 4.10.

Several things should be stressed out. First, looking at the density distribution in Figure 4.2, the criteria HR1 > 0.2 might be useful to discriminate COs and AGNs. The problem with this arises from the high difference in the number of AGNs and COs in the 1SXPS catalog. This will lead to a retrieved CO sample that will contain a large fraction of AGNs. Therefore, to isolate AGNs, but also to decrease the probability of missing COs, the variability and spatial distribution criteria described above were applied to the whole HR1 > 0.0 area. In addition, I stress that several combination of the selection rules and several orders to apply them were tried. One of the considered selection criteria was based on expectation that different percentages of AGNs, COs and stars have different values of the logarithm of the X-ray flux. Some other investigated properties included the behavior of variability P_{OBS} or $P_{SN} < 0.05$, as its dependence on the number of counts in respective bands. However, these criteria did not improve the results of the classification scheme. At the end, the selection rules that gave the best result were applied and described here (Figure 4.10).

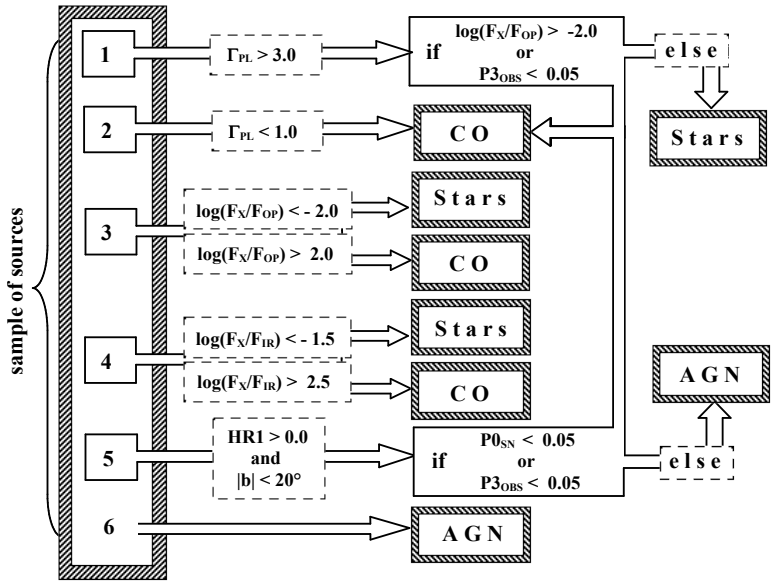

Figure 4.10: Flowchart showing the selection process. Numbers display the order of application of the selection rules on the sample of sources.

The derived classification scheme was applied to the golden sample in order to test the robustness and reliability of the defined selection criteria and to make some adjustments if necessary. This results in a retrieval fraction of around 90% for stars, 38% for COs, and 93% for AGNs. The probability that the source has been wrongly classified, defined as the ratio between the number of false identifications to the total number of identified sources, is 26% for the stars, 78% for the COs and 10% for the AGNs. Taken into account that not all objects have calculated quantities used in the selection criteria scheme (e.g., less than a half of AGNs and less than 20% of stars have Γ_{PL}-values provided), the applied selection scheme enables to classify correctly most of the stars and AGNs.

From the objects retrieved as CO candidate, 56% of that sample are in fact AGNs. Interestingly, although a lot of the CO and AGN properties overlap, the selection criteria isolated only 4% of AGNs as COs, and the CO high false identification rate is due to the large difference in population between AGN and COs in the golden sample. The retrieved percentage of COs

and its false identification rate are then in accordance with the prediction stated before (<5% of AGNs will be selected as COs). As seen in Table 3.1, 6 of the 16 catalogs used for the cross-correlation with the 1SXPS catalog were CO-class based, and the 2 star catalogs also contained COs. Therefore I think that this difference in numbers is not due to the incompleteness in the CO class caused by the small number or poorly chosen catalogs. For comparison, Lin et al. (2012), considering only a sample of bright *XMM-Newton* sources, obtained 70% of retrieved COs with a false identification probability of 18% when applying their selection rules on already identified sources. While the number of identified COs from the cross-correlation and literature is equal to 138 in Lin et al. (2012), and for the golden sample in the present work it is equal to 233, the difference is larger for AGNs. Lin et al. (2012) found 753 AGNs from the external catalog cross-correlation, while there is 4929 AGNs in the golden sample. Note that a high number of AGNs has the disadvantage of causing high false identification rate for stars and COs, but the advantage of favoring low false identification rate for the AGN group.

One can argue that AGN candidates should not be (partially) retrieved just on the basis that they correspond to the remaining uncategorized sources, but that the selection rules should be based on their properties. Indeed, 51% of the AGN group is obtained with just taking the sources that where not selected by any of the applied rules. But, if the value range of the AGN spectral and spatial property distributions is examined, it can be seen that these intervals are the ones left unselected. For example, the contribution to the false identification probability remains the same if we consider just the AGNs selected by the HR1 < 0.0 condition. In the retrieved golden sample of AGNs, there were also 167 ordinary galaxies and 105 galaxy clusters, meaning that in average 63% of galaxies and galaxy clusters from the golden sample were selected as AGNs. From this I can conclude that galaxies share similar investigated properties with AGNs. This does not necessarily increase the true false identification rate for AGNs. Completeness of the galaxy catalogs used for the cross-correlation with the 1SXPS clean sample is high (Paturel et al. 2005, Sanders et al. 2003), and only 361 ordinary

galaxy were found. Also, 14 of 17 SNRs were classified as AGNs, but that does not significantly affect the false identification rate for AGNs.

The average properties of the different classes of objects are also consistent with what we know from literature. The inconsistency of the density distribution of stars in the HR1-HR2 diagram with the rest of the results can raise a question about the validity of the products discussed above, and therefore the validity of the derived criteria for this work. Although the nature of this inconsistency is still unknown, I am confident about the reliability of the overall obtained results and the derived selection criteria. All products except the one reported for stars (the color-color diagram) are consistent with the results obtained by Lin et al. (2012) who followed the same methodology. As it is pointed out in Section 4.4, our results and theirs are remarkably similar, but some deviations are to be expected because of the differences in the energy band coverage, spectral response or data processing.

4.4 Classification of the 1SXPS sources from the clean sample

The selection rules described in Section 4.3 were applied to the rest of the 1SXPS clean sample. As a result, 78,918 objects were classified as AGN candidates, 9294 as star candidates and 3752 as CO candidates. The same spectral, temporal and spatial products as for the golden sample were built in order to compare them. Then the observed differences and similarities can be used to make a conclusion about the validity of the obtained classification.

4.4.1 Spatial distribution

Figure 4.11 shows the distribution of candidate objects with respect to the Galactic latitude b. The AGN candidates show a bimodal distribution, as in the case of the golden sample group, with a minimum in the area of the Galactic plane due to the high Galactic absorption at these latitudes. In opposite, stars tend to concentrate at low Galactic latitudes, and show a maximum in this area. While these two distributions provide a good

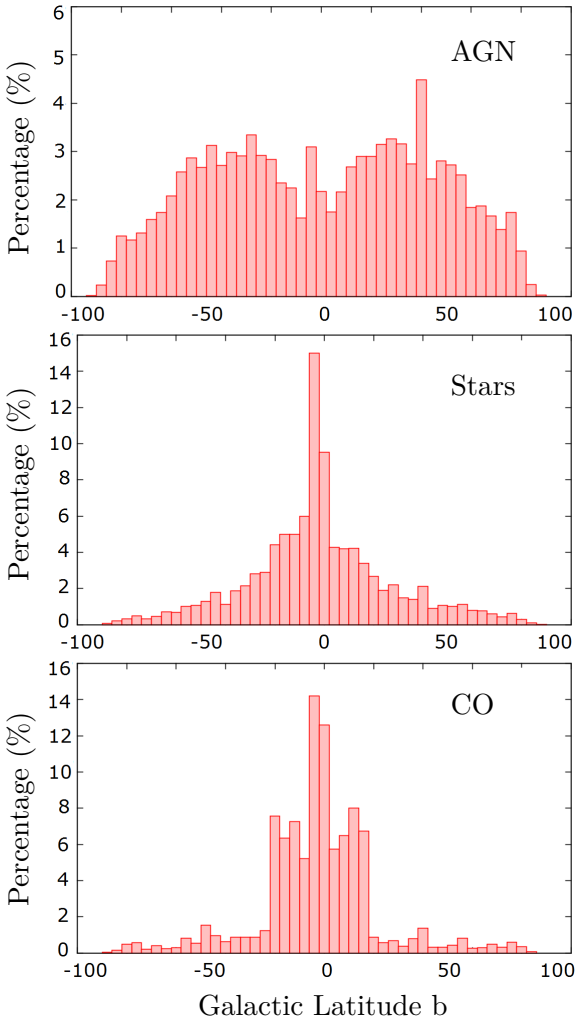

Figure 4.11: Distribution of sources for the AGN, star and CO candidates as a function of the Galactic latitude. Note that bin sizes do not correspond to the equal spatial area.

indicator of the successful application of the selection rules, COs distribution is a direct consequence of the selection rules. The effect of the $|b| < 20°$ conditions can be seen with the sharp increase in the population of CO candidates in that area. These results show remarkable similarity to the golden sample distributions, although there was no selection rule based on the Galactic latitude for AGNs and stars. The increase in the number of

objects at $b = 0^{\circ}$ is common to all three groups, and can be explained by the pointing overdensity of the *Swift* mission in the area of the Galactic center (a result of a large program to monitor the long-term X-ray behavior of the central super massive black hole Sgr A$*$).

4.4.2 Spectral properties

Figure 4.12 (left) shows the density distribution of candidate sources on the color-color diagram. AGN candidates exhibit the same shape and location as seen in the case of the golden sample, i.e. concentrating in the middle of the diagram. Stars again form the moon-like shape, with the highest density found in the region of the HR1-HR2 diagram where kT temperatures predicted by the APEC model could be found. COs occupy the right part of the plot. The distribution shape is in agreement with the traced by a wide range of the Γ_{PL}-values (see Figure 4.6 in Section 4.2). The sudden drop in the density map for COs below 0.0 is due to the AGN selection rule.

The Γ_{PL}-distribution for AGN, stars and COs is shown in Figure 4.12 (right). The Gaussian function that I obtained from the AGN golden sample distribution is plotted for reference in the three cases. The retrieved distributions are similar to those obtained from the golden sample. The Γ_{PL}-values for AGNs peaks around 1.7. This is consistent with what I found using the golden sample and what could be found in the literature. The two minima in the CO distribution are due to the cutoffs in the selection rules. I used all the available Γ_{PL}-values when applying the selection rules, but I only considered the ones with a good fit to do the plot. Using all the Γ_{PL}-values does not make a significant difference in the distribution shape.

Looking at Figure 4.13, we see that stars for both X-ray to optical (left) and X-ray to IR (right) flux ratios have the smallest values of these three groups, as expected. The distribution of AGN candidates has a similar shape to that observed for the golden sample, but without the long tail down to the lower ratio values. This is a result of the selection rules. The distribution for CO candidates are consistent with those seen for the golden sample, expect that I find a higher number of objects with low values of the X-ray to optical flux ratio. This may be partially due to a possible contamination

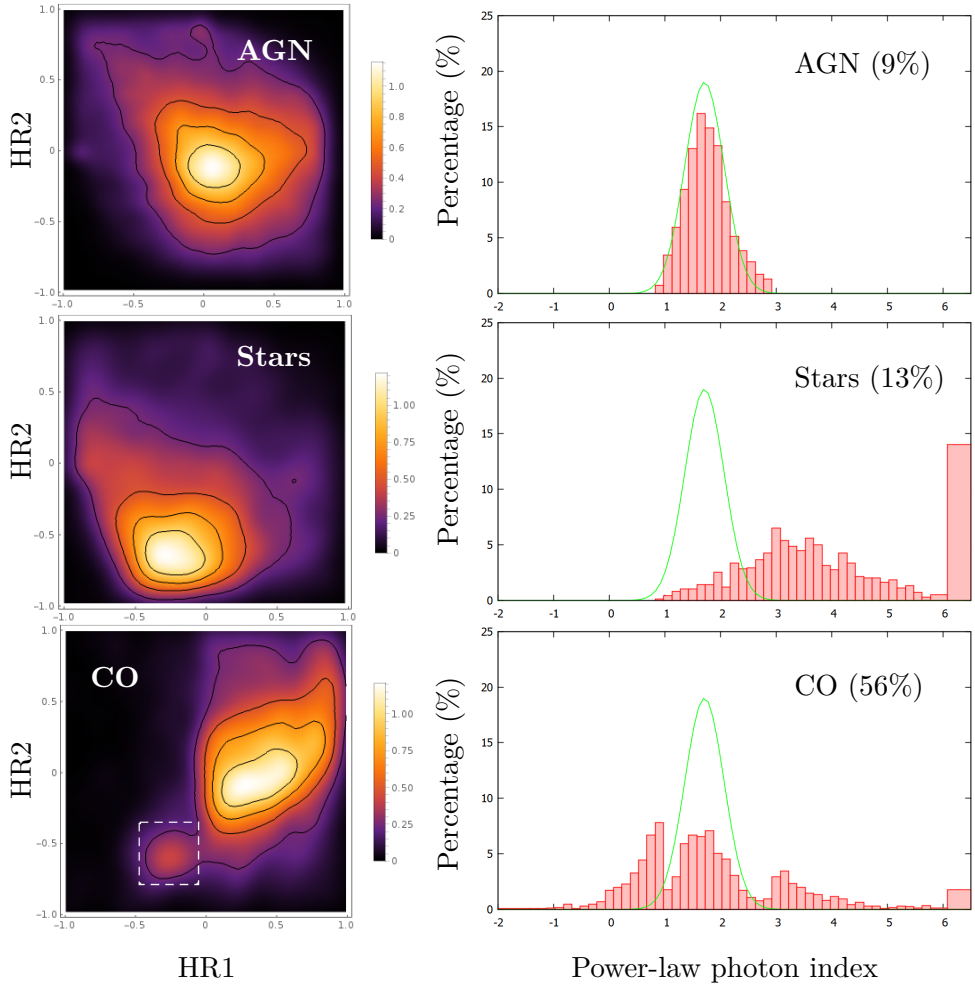

Figure 4.12: Left - X-ray color-color diagrams for the AGN, star and CO candidates. Because of the large number of sources, the color-color diagrams show the source density distribution in arbitrary units. The dashed square, which encloses a sample of CO candidates, is plotted for reference. Right - Distribution of the power-law photon index (Γ_{PL}) for the same source candidates. A normal distribution with a mean of 1.71 and a standard deviation of 0.35 obtained from the golden sample is plotted for reference. The Γ_{PL}-values considered are the ones with reduced χ^2 between 0.6 and 1.5. Values of the photon index greater than 6.0 are placed into one bin. In parentheses, I provide the percentage of AGN, star and CO candidates for which the Γ_{PL}-values are available, regardless of the reduced χ^2-value.

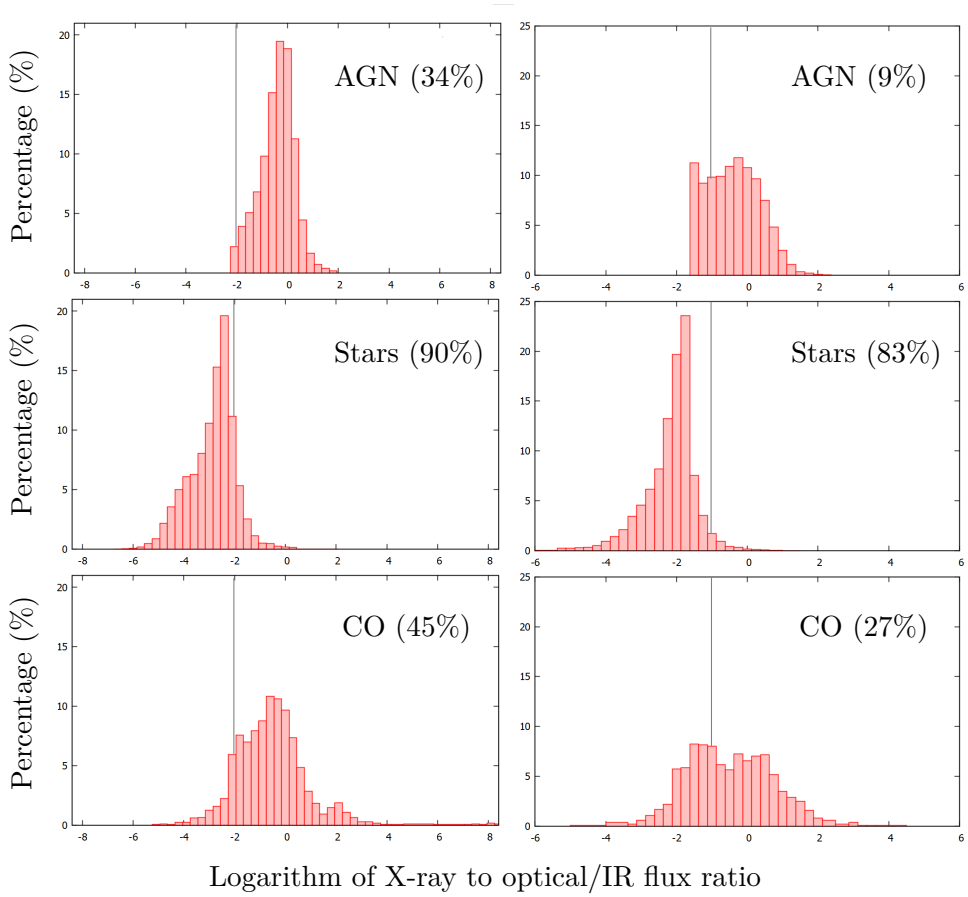

Figure 4.13: Left - Distribution of the X-ray to optical flux ratios for the AGN, star and CO candidates. Vertical solid line plotted for reference is the same as the one in the golden sample distribution. The optical fluxes were derived from the USNO B1.0 $R2$ or $R1$ magnitude. Right - Distribution of the X-ray-to-infrared flux ratios for the same candidate sources. Vertical solid line is plotted for reference as in the golden sample. The infrared fluxes were derived from the 2MASS K_S magnitude. In parentheses, I provide the percentage of AGN, star and CO candidates for which the plotted quantities are available.

in this range with stars and AGNs (or it might also be the case of XRBs in the low/hard state). This can also be seen in the distribution regarding IR counterparts, where the CO and AGN candidate distribution peak have shifted to the left in comparison with the golden sample distributions. Star candidates in general have more narrower X-ray to IR flux ratio distribution than the ones computed in the golden sample. The distribution shape for AGNs also shows contamination with other source types. This does not necessarily mean that the level of the false identification rate for AGN candidates corresponds to the percentage of AGN candidates with low values of the X-ray to IR flux ratio. While in the golden sample 53% of all objects had IR counterparts, for the rest of the 1SXPS clean sample that value drops to 17%. Indeed, while the percentage of star candidates with provided IR counterpart is still reasonable high (83%), the percentage of the AGN candidates with IR counterparts is only 9% (while for the golden sample AGNs it was 42%). Therefore, the plotted values and the distribution shape can not be considered as representative of the whole AGN candidate sample.

4.4.3 Temporal properties

Variability products for the candidate objects are shown in Figure 4.14. The distribution of $P0_{SN}$ and $P3_{OBS}$ for AGN and star candidates does not significantly differ. The CO candidate sample show strong variability, with 54% of the objects with $P0_{SN} < 0.05$ and 59% with $P3_{OBS} < 0.05$. The result is partially the consequence of the selection rules established in Section 4.3. Excluding the subgroups of COs isolated by the selection rules based on $P0_{SN}$ and $P3_{OBS}$ (second to last bullet point in Section 4.3), I still find that the final CO candidates exhibit larger variability than AGNs and stars. More precisely, 34% and 28% of CO candidates would still have $P0_{SN}$ and $P3_{OBS}$ less than 0.05. This is to be compared to 11% and 8% of AGNs and 20% and 10% of star candidates that have $P0_{SN}$ and $P3_{OBS} < 0.05$, as shown in Figure 4.14.

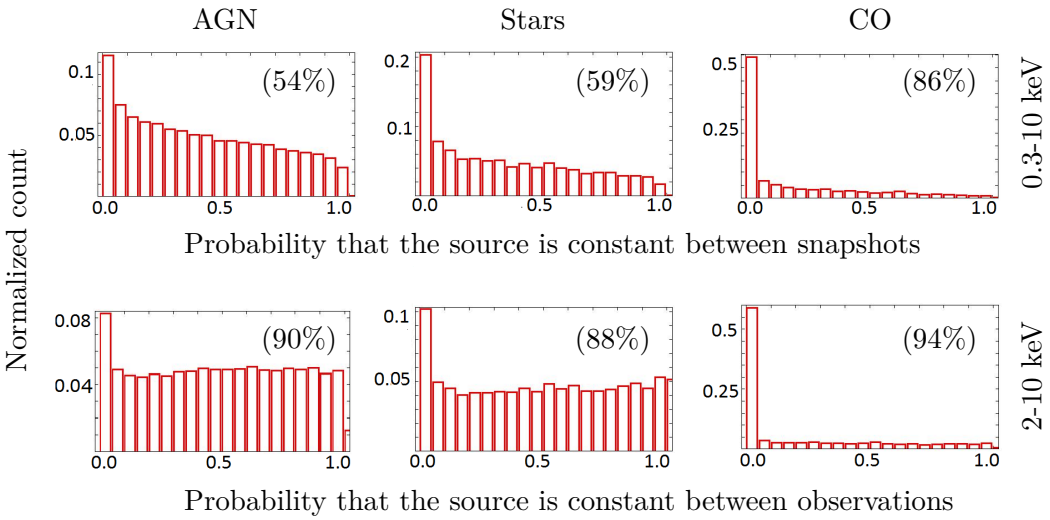

Figure 4.14: Probability that the source is constant from snapshot to snapshot (top panel) in the total band (0.3 – 10 keV) and from observation to observation (bottom panel) in the hard band (2 – 10 keV), for candidate sources. On the y-axis is shown the normalized number of sources of a given type. In parentheses, I provide the percentage of AGN, star and CO candidates for which the plotted quantities are available.

4.4.4 Additional verifications

I performed several investigations on a subsample of the resulting candidate groups in order to validate or discard the type identification of these objects. The X-ray to optical flux ratio distribution for the small candidate CO bulk (the dotted box in Figure 4.12), was compared with both the one from the whole candidate CO sample, and the one that corresponds to star candidates. The bulk contains 7% of the CO candidates group, and its distribution of X-ray to optical flux ratio is shifted to the left, with the peak at -2, showing the possible contamination with stars. In favor of this possibility is the fact that 80% of the objects in it have optical counterparts, while when considering the whole CO candidates sample that value drops to 45%. Also, the properties of the AGN candidates were investigated in more detail in order to search for possible star contamination. Namely, AGN

candidates with $|b| < 20^\circ$ were divided into two groups, named Sagittarius and Not Sagittarius, separated by the value of the Galactic longitude l as follows:

$$\text{Sagittarius:} \quad l \in [0^\circ, 90^\circ] \cup [270^\circ, 360^\circ]$$
$$\text{Not Sagittarius:} \quad l \in [90^\circ, 270^\circ]$$

The Sagittarius group then represents the AGN candidates with high probability of star contamination in contrast to the Not Sagittarius one, as these sources are on the side that is faced to the Galactic center where most of the stars reside. The possible contamination should then emerge as the difference in the properties of these two groups. Various quantities were plotted, including the HR1-HR2 distribution, Γ_{PL}-values and X-ray to optical/IR flux values in order to search for differences between the two groups and to compare the results with the whole candidate AGN sample. No significant differences were observed.

The *Swift*-BAT catalog (Baumgartner et al. 2013) is a result of 70 months of observations of the BAT hard X-ray detector. It contains 1171 hard X-ray sources in the 14 – 195 keV band, associated with 1210 counterparts (with Right Ascension and Declination usually taken from NED or SIMBAD). As the catalog provides source type classification, cross-correlating it with the *Swift*-XRT AGN, star and CO candidates offers a way to check the robustness of the obtained false identification rate. Cross-correlation with AGN candidates resulted in 115 counterparts, from which 59 were also classified as AGNs in the *Swift*-BAT catalog, giving the false identification probability of 49%. If sources categorized as *Unknown* in the *Swift*-BAT catalog are also considered as valid source-type match, the false identification probability drops to 40%. For star candidates cross-match resulted in 31 BAT counterparts, but none was classified as star in the *Swift*-BAT catalog. Because of the hard X-ray band, contamination in the star candidate group could have been selected in a biased way. The CO candidates have 155 BAT counterparts, with false identification probability of 67% or 50% if the sources designated as *Unknown* in the *Swift*-BAT catalog are also considered.

One of the columns in the 1SXPS catalog shows the number of found matches for the given source in one of the 13 catalogs and databases used by Evans et al. (2014). There are 11,509 sources in the 1SXPS clean sample with no match within any of the catalogs used in Evans et al. (2014) work. Looking at the 78,918 candidate AGNs, stars and COs from this work, there is in total 11,499 sources that were not found in any of the catalogs used for cross-correlation in both researches. These 9 star candidates, 122 CO candidates and 11,368 AGN candidates form a valuable group of possibly, until now, unobserved new sources.

5 Conclusion and perspectives

The main goal of this project was to find a way to identify the nature of the X-ray sources within the *Swift*-XRT catalog using timing, spatial and spectral information provided within it, coupled with multi-wavelength data from external catalogs. Once the general behavior of AGNs, CO and stars was investigated on a subsample of identified sources, made conclusions were used to derive the selection criteria, which return classified the remaining sources in the 1SXPS catalog. This required processing large databases of sources and understanding the way in which the source properties are calculated and how the final catalog is formed. Sampling AGNs can give us further insight into the formation of galaxies and how they co-evolved with SMBHs. Demographic studies of stellar-mass COs can be used to explore both past and ongoing star formation. Interesting sources can then be further used to study matter in extreme conditions and to test fundamental physics by observing the phenomena that arise in strong gravitational fields. This in return can reveal regimes of physics that can not be tested elsewhere. Because of this, it is important to exploit available X-ray catalogs such as 1SXPS and find new, until now unobserved sources.

The 1SXPS catalog clean sample was cross-matched with 16 external multi-wavelength catalogs that provided objects classification. As a result, 6798 sources from the clean sample were identified, mostly as AGNs and stars. There are also 231 COs, divided into subclasses of ULXs, CVs and XBs. They tend to be extremely variable, more than AGNs and stars. Among the studied properties of the three different classes of objects, the distribution with respect to the Galactic latitude is the only one common

to stars and COs together, as the objects are concentrated in the Galactic plane in both cases. AGNs, as extragalactic sources, should have uniform distribution, but due to the Galactic absorption and sky coverage of AGN surveys, this group has a low number of sources at low galactic latitudes. Their power-law photon index distribution peaks around 1.7, and has the shape of a Gaussian function. Stars tend to have softer spectra, with the majority having $\Gamma_{PL} > 3$. The Γ_{PL}-distribution of COs is widely spread, a result in agreement with spectral state transitions often seen in these type of objects (hard and soft states), depending on the regime of accretion. Based on these properties, I defined classification criteria. When applied back to the golden sample, 73% of the stars, 35% of the COs, and 95% of the AGNs were retrieved. The low number of COs and their high probability of false identification (78%) is due to the large number of AGNs in the sample with which they share similar properties. When the selection rules were applied to the rest of the 1SXPS clean sample, 78,918 objects were classified as the AGN candidates, 9294 as the star candidates and 3752 as CO candidates. The three obtained groups share similar properties with the corresponding groups from the golden sample, and by that represent valuable group of objects for future studies.

Perspectives for this work are numerous. Base of identified sources and products that was made can be widely explored and exploit in order to find new previously unstudied sources with interesting characteristics. Any sources with extreme values of one of the products, that deviate from the class average, suggest a possible contamination with other class type or an unusual source with interesting properties. Then these sources can be further investigated with building per source products, such as spectra or light curves. For example, a very soft source classified as AGN would indicate a possible TDE. More knowledge about the three main types can be gained by investigation of their subclasses behavior by building the same products. Studying the differences between the subclasses such as CV, XBs, isolated WD or ULXs can offer a way to define new selection criteria which would target a specific subclass based on its distinctive properties, thous improving its false identification rate. Additionally, cross-correlating the 1SXPS catalog

with galaxy catalogs in search for the source not coincident with the nucleus of the galaxy, exhibiting properties similar to the ULX subclass, could lead to new IMBH candidates. The same cross-correlation can be used to find AGN-like sources in dwarf galaxies, which could also harbor an elusive IMBH. Sampling the fraction of small galaxies that contain massive black holes will enable the distinction between two SMBH formation mechanisms, and give further insight to BH and the host galaxy co-evolution.

Except the exploitation of obtained results, there are still different ways to check the reliability of the derived selection scheme or investigate the possible improvements. UVOT and BAT data provide additional information on the per source basis. This access to multiwavelength data is one of many advantages of the *Swift* mission as it provides several strategies to tackle the problem. The *Swift*-XRT light curves can be used to compute variability indicator more efficient than the one provided in the 1SXPS catalog. Including such variability indicator would help to improve the classification of COs. The group of candidate sources, together with the investigation of interesting objects, could result in a list of objects for which the further multi-wavelength observations would be requested.

References

Ayal, S., Livio, M., & Piran, T. 2000, ApJ, 545, 772

Aird, J., Comastri, A., Brusa, M., et al. 2013, An Athena+ supporting paper: The formation and growth of the earliest supermassive black holes, 2013arXiv1306.2325

Anderson, E., & Francis, C. 2012, Astronomy Letters, 38, 331

Anderson, W. 1929, Z. Phys. 1, 851

Antonucci, R. 1993, ARA&A, 31, 473

Baade, W., & Zwicky, F. 1933, Phys Rev, 46, 76

Bachetti, M., Harrison, F. A., Walton, D. J., et al. 2014, Nature, 514, 202

Bade, N., et al. 1996, A&AS., 309, L35

Balázs, L. G., Mészáros, A., & Horváth, I. 1998, A&A, 339, 1

Balman, S. 2012, Memorie della Societa Astronomica Italiana, 83, 585

Barcons X., et al., Athena (Advanced Telescope for High ENergy Astrophysics) Assessment Study Report for ESA Cosmic Vision 2015-2025 ArXiv e-prints (2012) :arXiv:1207.2745

Barret et al. 2013, SF2A, 237-243

Barth, A. J., Sarzi, M., Rix, H.-W., Ho, L. C., Filippenko, A. V., & Sargent, W. L. W. 2001, ApJ, 555, 685

Barthelmy, S. D., et al. 2005, Space Sci. Rev., 120, 143

Baumgartner, W. H., Tueller, J., Markwardt, C. B., et al. 2013, ApJS, 207, 19

Belczynski, K., Bulik, T., Fryer, C. L., et al. 2010, ApJ, 714, 121

Bethe, H. A. 1990, Rev. Mod. Phys. 62, 801

Bethe, H. A., & Wilson, J. R. 1985, ApJ, 295, 14

Bloom J. S., Giannios D., Metzger B. D., et al. 2011, Science, 333, 203

Bolton, CT 1972. Nature 235: 271-73

Brenneman, L. W., & Reynolds, C. S. 2006, ApJ, 652, 1028

Bromm, V., & Yoshida, N. 2011, ARA&A, 49, 373

Brown, G. E., & Bethe, H. A. 1994, ApJ, 423, 659

Burrows, D. N., Hill, J. E., Nousek, J. A., et al. 2005, Space Sci. Rev., 120, 165

Burrows D. N., et al. 2011, Nature, 476, 421

Caccianiga, A., et al. 2004, A&A, 416, 901

Cappelluti, N., et al. 2009, A&A, 495, L9

Cappi, M., Done, C., Behar, E., et al. 2013, An Athena+ supporting paper: Astrophysics of feedback in local AGN, 2013arXiv1306.2330

Carrol, B. W., & Ostlie, D. A. 2007, An Introduction to Modern Astrophysics, 75, 483, 653, 1085

Chandrasekhar, S. 1931, ApJ, 74, 81

Chisholm, J. R., Dodelson, S., & Kolb, E. W. 2003, ApJ, 596, 437

Chomiuk, L., & Wilcots, E. M. 2009, ApJ, 703, 370

Cohen, M., Wheaton, W. A., & Megeath, S. T. 2003, AJ, 126, 1090

Colbert, E., & Mushotzky, R. 1999, ApJ, 519, 89

Corral, A., Della Ceca, R., Caccianiga, A., Severgnini, P., Brunner, H., Carrera, F. J., Page, M. J., Schwope, A. D. 2011, A&A, 530, A42

Cowley, A.P., Crampton, D., Hutchings, J.B., Remillard, R., Penfold, J.E. 1983, Ap. J. 272: 118-22

Croston, J. H., Sanders, J. S., Heinz, S., et al. 2013, An Athena+ supporting paper: AGN feedback in galaxy clusters and groups, 2013arXiv1306.2323

Cutri et al. 2003, AJ, V131, Iss2, pp 1163-1183

D'Elia, V., Perri, M., Puccetti, S., et al. 2013, A&A, 551, A142

Davis, S. W., Narayan, R., et al. 2011, ApJ, 734, 111

Devecchi, B., & Volonteri, M. 2009, ApJ, 694, 302

Done, C., Davis, S. W., Jin, C., Blaes, O., & Ward, M. 2012, MNRAS, 420, 1848

Donley, J. L., Brandt, W. N., Eracleous, M., & Boller, T. 2002, ApJ, 124, 1308

Dovciak, M., Matt, G., Bianchi, S., et al. 2013, An Athena+ supporting paper: The close environments of supermassive black holes, 2013arXiv1306.2331

Eckart, A., & Genzel, R. 1996, Nature, 383, 415

Eichler, D., Livio, M., Piran, T., et al. 1989, Nature, 340, 126

Elvis, M., Page, C. G., Pounds, K. A., Ricketts, M. J., Turner, M. J. L. 1975. Nature 257: 656-57

Epstein, R.I. 1979, MNRAS, 188, 305

Esquej, P., Saxton, R. D., Komossa, S., et al. 2008, A&A, 489, 543

Ettori, S., Pratt, G. W., de Plaa, J., et al. 2013, An Athena+ supporting paper: The astrophysics of galaxy groups and clusters, 2013arXiv1306.2322

Evans, P. A., et al. 2009, MNRAS, 397, 1177

Evans, P. A., Osborne, J. P., Beardmore, A.P., et al. 2014, ApJ, v. 210, article id. 8, 24 pp

Evans, I. N., Primini, F. A., Glotfelty, K. J., et al. 2010, ApJS, 189, 37

Fabbiano, G. 1989, ARA&A, 27, 87

Fabbiano, G. 1995, in X-Ray Binaries, W. H. G. Lewin, J. van Paradijs & E. P. J. van den Heuvel, eds. (CUP: Cambridge), 390-416

Fabbiano, G. 2002, ASPC, 253, 93F

Fabian, A. et al., arXiv: 0903.4424 (2009)

Fabian A. C., 2012, ARA&A, 50, 455

Fan, X., et al. 2001, AJ, 122, 2833

Farrell, S. A., Webb, N. A., Barret, D., Godet, O., Rodrigues. J. M. Nature 460 (7251), 73-75

Feng, H., Soria, R. 2011, New A Rev., 55, 166

Ferrarese, L., & Merritt, D. 2000, ApJ, 529, L9

Fleming, T. A., Snowden, S. L., Pfeffermann, E., Briel, U., Greiner, J. 1996, AA 316, 147

Fontaine, G., Brassard, P., & Bergeron, P. 2001, PASP, 113, 409

Frank, J., King, A., & Raine, D. 1992, Accretion Power in Astrophysics, Cambridge University Press, Cambridge

Gebhardt, K., et al. 2000, ApJ, 539, L13

Gehrels, N., Chincarini, G., Giommi, P., et al. 2004, ApJ, 611, 1005

Genzel, R., Crawford, M. K., Townes, C. H., & Watson, D. M. 1985, ApJ, 297, 766

Georgakakis, A., Carrera, F., Lanzuisi, G., et al. 2013, An Athena+ supporting paper: Understanding the build-up of supermassive black holes and galaxies at the heyday of the Universe, 2013arXiv1306.2328

Ghez, A. M., Klein, B. L., Morris, M., & Becklin, E. E. 1998, ApJ, 509, 678

Ghez, A. M., Morris, M., Becklin, E. E., Tanner, A., & Kremenek, T. 2000, Nature, 407, 349,

Giacconi, R., et al. 1979, ApJ, 230, 540

Giammichele, N., Bergeron, P., & Dufour, P. 2012, ApJS, 199, 29

Gladstone, J. C., Roberts, T. P., Done, C. 2009, MNRAS, 397, 1836

Godet, O., Plazolles, B., Kawaguchi, T., Barret, D., Webb, N.A., et al 2012, ApJ, 752, 34

Graham, A. W., Erwin, P., Caon, N., & Trujillo, I. 2001, ApJ, 563, L1

Greene, J. E. 2012, Nature Communications, 3, 1304

Grupe, D., Thomas, H.-C., & Leighly, K. M. 1999, A&A, 350, L31

Gurzadian V. G., Ozernoi L. M., 1981, A&A, 95, 39

Haehnelt, M. G., & Rees, M. J. 1993, MNRAS, 263, 168

Heger, A., Fryer, C. L., Woosley, S. E., Langer, N., & Hartmann, D. H. 2003, ApJ, 591, 288

Herrnstein, J. R., Moran, J. M., Greenhill, L. J., & Trotter, A. S. 2005, ApJ, 629, 719

Ho, L. C. 2008, ARA&A, 46, 475

Ho, L. C., Filippenko, A. V., & Sargent, W. L. W. 1997, ApJS, 112, 315

Holberg, J. B., Sion, E. M., Oswalt, T., et al. 2008, AJ, 135, 1225

Horváth, I., Balázs, L. G., Bagoly, Z., Ryde, F., Mészáros, A. 2006, A&A, 447, 23

Huwyler, C., Porter, E. K., and Jetzer, P. 2015, Phys.Rev. D91, 024037

Jansen, F., Lumb, D., Altieri, B., et al. 2001, A&A, 365, L1

King, A. R., Davies., M. B., Ward, M. J., Fabbiano, G., & Elvis, M. 2001, ApJ, 552, L109

Kleinman, S. J. 2010, in Werner K., Rauch T., eds, AIP Conf. Ser. Vol. 1273, 17th. European White Dwarf Workshop. Am. Inst. Phys., New York, p.156

Komossa, S. 2002, Reviews in Modern Astronomy, 15, 27

Komossa, S. 2012, EJP Web Conferences, 02001

Komossa, S., & Bade, N. 1999, A&AS, 343, 775

Komossa, S., & Greiner, J. 1999, A&A, 349, L45

Kormendy, J., & Ho, L. C. 2013, ARA&A, 51, 511

C., Kouveliotou 1999, Magnetars, Proceedings of the National Academy of Science, 96, 5351-5352

Kuo, C. Y., et al. 2011, ApJ, 727, 20

Lacy, J. H., Townes, C. H., Geballe, T. R., & Hollenbach, D. J. 1980, ApJ, 241, 132

Landau, L. 1932, Phys. Z. Sowjetunion 1, 285

Lasota, J.-P. 2001, New Astronomy Review, 45, 449

Li, Y., et al. 2007, ApJ, 665, 187

Lin, D., Carrasco, E. R., Grupe, D., Webb, N. A., Barret, D., Farrell, S. A. 2011, ApJ, 738, 52

Lin, D., Smith, I. A., Liang, E. P., Bridgman, T., Smith, D. M., Martí, J., Durouchoux, P., Mirabel, I. F., & Rodríguez, L. F. 2000, ApJ, 532, 548

Lin, D., Webb, N. A., Barret, D. 2012, ApJ, 756, 27

Liu, J., Bregman, J. N., Bai, Y., Justham, S., & Crowther, P. 2013, Nature, 503, 500

Liu, Q. Z., & Mirabel, I. F. 2005, A&A, 429, 1125

Lopes de Oliveira, R., Motch, C., Smith, M. A., Negueruela, I., & Torrejón, J. M. 2007, A&A, 474, 983

Maccacaro, T., Gioia, I. M., Wolter, A., Zamorani, G., & Stocke, J. T. 1988, ApJ, 326, 680

MacFadyen, A. I., & Woosley, S. E. 1999, ApJ, 524, 262

Maksym, W. P., Ulmer, M. P., Eracleous, M. 2010, ApJ, 722, 1035

Merritt, D., Milosavljevic, M., Favata, M., Hughes, S. A., & Holz, D. E. 2004, ApJ, 607, L9

Middleton, M. J., et al. 2013, Nature, 493, 187

Miller, M. Coleman, Colbert, E. J. M. 2004, International Journal of Modern Physics D, 13, 1

Monet, D. G., Levine, S. E., Canzian, B., et al. 2003, AJ, 125, 984

Motch, C., Pakull, M. W., Soria, R., Gris, F., & Pietrzyski, G. 2014, Nature, 514, 198

Nandra, K., & Pounds, K. A. 1994, MNRAS, 268, 405

Narayan, R., Garcia, M. R., & McClintock, J. E. 1997, ApJ, 478, L79

Ochsenbein, F., Bauer P., Marcout, J., A&AS, v.143, p.23-32

Oppenheimer, J. R., & Snyder, H. 1939, Phys. Rev. 56, 455

Oppenheimer, J. R., & Volkoff, G. M. 1939, Phys. Rev. 55, 374

Paris, I. et al. 2012, A&A, 548, 66

Paturel, G., Vauglin, I., Petit, C., Borsenberger, J., Epchtein, N., Fouqué, P., & Mamon, G. 2005, A&A, 430, 751

Pearson, K. 1900, Philosophical Magazine Series 5, 50, 157

Pringle., J.E. 1981, ARA&A, 19: 137-162

Pringle, J. E., & Wade, R. A., editors. Interacting binary stars. Cambridge University Press, Cambridge, 1985

Pointecouteau, E., Reiprich, T. H., Adami, C., et al. 2013, An Athena+ supporting paper: The evolution of galaxy groups and clusters, 2013arXiv1306.2319

Portegies Zwart, S. F., Baumgardt, H., Hut, P., Makino, J., & McMillan, S. L. W. 2004, Nature, 428, 724

Psaltis, D., Ozel, F., Chan, C.-K., & Marrone, D. P. 2014, arXiv:1411.1454

Puccetti, S., Capalbi, M., Giommi, P., et al. 2011, A&A, 528, A122

Rasio, F. A., et al. 2006, in van der Hucht K.A., ed., Highlights of Astronomy Vol. 14, Proc. XXVIth IAU General Assembly

Raymond, J. C. 2005, AIP Conf. Proc. 774, 15

Rees, M. J. 1988, Nature, 333, 523

Remillard, R. A., & McClintock, J. E. 2006, ARA&A, 44, 49

Reynolds, C. S., & Fabian, A. C. 2008, ApJ, 675, 1048

Richstone, D., et al. 1998, Nature, 395, A14

Risaliti, G., Maiolino, R., Salvati, M. 1999, ApJ, 522, 157

Ritter, H., Kolb, U. 2003, A&A, 404, 301 (update RKcat 7.21, 2013)

Roberts, T. P. 2007, Astrophysics and Space Science, 311, 203

Romano, P., Campana, S., Mignani, R. P., et al. 2008, A&A, 488, 1221

Roming, P. W. A., et al. 2005, Space Sci. Rev., 120, 95

Rosen et al. 2015, submitted to A&A, arXiv:1504.07051v2

Sadat, R., Blanchard, A., Kneib, J.-P., Mathez, G., Madore, B., & Mazzarella, J. M. 2004, A&A, 424, 1097

Salaris, M., García-Berro, E., Hernanz, M., Isern, J., & Saumon, D. 2000, ApJ, 544, 1036

Samus, N.N., Durlevich, O.V., Kazarovets, E V., et al., General Catalog of Variable Stars, VizieR Online Data Catalog, Version 2012Apr

Sanders, D. B., Mazzarella, J. M., Kim, D.-C., et al. 2003, AJ, 126, 1607

Santos-Lleo, M., et al. 2009, Nature 462, 997

Satyapal, S., Vega, D., Heckman, T., O'Halloran, B., & Dudik, R. 2007, ApJ, 663, L9

Saxton, R. D., Read, A. M., Esquej, P., Komossa, S., Dougherty, S., Rodriguez-Pascual, P., Barrado, D. 2012, A&A, 541, A106

Schwarzschild, K., Sitzungsber. Preuss. Akad. Wiss., Phys. Math. Kl. 1916, 189 (communicated 13 Jan. 1916)

Servillat, M., Farrell, S. A., Lin, D., Godet, O. Barret, D., Webb, N. A. 2011, ApJ, 740

Singh, K. P., Garmire, G.P., & Nousek, J. 1985, ApJ, 297, 633

Skrutskie, M. F., Cutri, R. M., Stiening, R., et al. 2006, AJ, 131, 1163

Smith, R. C. (2006, November). Cataclysmic variables. Contemporary Physics 47, 363-386

Smith, R. K., Brickhouse, N. S., Liedahl, D. A., & Raymond, J. C. 2001, ApJ, 556, L91

Straub, O., Godet, O., Webb, N.A., Servillat, M., Barret, D. 2014, A&A, 569, 116

Strubbe, Linda E., Quataert, Eliot 2009, MNRAS, Volume 400, Issue 4, pp. 2070-2084

Tanaka, Y. 2000, in Highly Energetic Physical Processes and Mechanisms for Emission fro m Astrophysical Plasmas, eds. P. C. H. Martens, S. Tsuruta, & M. A. Weber, IAU Symp., 195, 37

Taylor, M, B., ASP Conf. Ser. 347, ADASS XIV, 29 (2005)

Treister, E., & Urry, C. M. 2005, ApJ, 630, 115

Trümper, J. 1983, Adv. Space Res. 2, No.4, 241

Turner, T.J., & Pounds, K.A. 1989, MNRAS, 240, 833

Turner, M. L., Rutledge, R. E., Letcavage, R., Shevchuk, A. S. H., & Fox, D. B. 2010, ApJ, 714, 1424

Ulmer, A. 1999, ApJ, 514, 180

Urosevic, D., Pannuti, T. G., Duric, N., Theodorou, A. 2005, A&A, 435, 437U

Urry, C. M., & Padovani, P. 1995, Publications of the Astronomical Society of the Pacific, 107, 803

van der Marel, R. P. 2004, in Coevolution of Black Holes and Galaxies, ed. L. C. Ho, Cambridge University Press, p. 37 (astro-ph/0302101)

van Wassenhove, S., Volonteri, M., Walker, M. G., & Gair, J. R. 2010, MNRAS, 408, 1139

Véron-Cetty, M., & Véron, P. 2010, A&A, 518, A10+

Voges, W., Aschenbach, B., Boller, T., et al. 1999, A&A, 349, 389

Volonteri, M. 2010, A&AR, 18, 279

Volonteri, M., Lodato, G., & Natarajan, P. 2008, MNRAS, 383, 1079

Walton, D. J., Roberts, T. P., Mateos, S., & Heard, V. 2011, MNRAS, 416, 1844

Wang, J., Merritt, D. 2004, ApJ, 600, 149

Watson, M. G., Schroder, A. C. Fyfe, et al. 2009, A&A, 493,339

Webster, B. L., Murdin, P. 1972, Nature 235: 37-38

Weisskopf, M. C., Tananbaum, H. D., Van Speybroeck, L. P., & O'Dell, S. L. 2000. Proc. SPIE, 4012, 2

Wen, Z. L., Han, J. L., & Liu, F. S. 2009, ApJS, 183, 197 –. 2012, ApJS, 199, 34

Woo, J.-H., & Urry, C. M. 2002, The Astrophysical Journal, 579, 530

Woosley, S. E., & Timmes, F. X. 1996, Nucl. Phys. A, 606, 137

Xue, Y. Q., et al. 2011, ApJS, 195, 10

Yakovlev, D. G., & Pethick, C. J. 2004, ARA&A, 42, 169